

## Chlorogenic acid-assisted dopamine-sodium alginate composite nanofiber membranes for promoting wound healing

Meng Zhang<sup>a</sup>, Yinchuan Wang<sup>a</sup>, Xueling Yin<sup>c</sup>, Mei Xue<sup>a</sup>, Xin Zhao<sup>a</sup>, Runxiao Zheng<sup>b,\*</sup>, Jianfeng Qiu<sup>a,\*</sup>, Zhihong Zhu<sup>c,\*</sup>

<sup>a</sup> Medical Engineering and Technology Research Center, School of Radiology, Shandong First Medical University, Shandong Academy of Medical Sciences, Tai'an 271000, China

<sup>b</sup> Medical Science and Technology Innovation Center, Shandong Provincial Hospital, Shandong First Medical University, Shandong Academy of Medical Sciences, Jinan 250000, China

<sup>c</sup> Institute of Nano-science and Nano-technology, College of Physical Science and Technology, Central China Normal University, Wuhan 430079, China



### ARTICLE INFO

**Keywords:**

Alginate  
Nanofiber membranes  
Chlorogenic acid  
Antioxidant  
Wound healing

### ABSTRACT

Developing safe and effective novel wound dressings to enhance full-thickness skin wound regeneration is highly desirable. In this study, we firstly incorporated chlorogenic acid (CA) into dopamine (DA) functionalized alginate (Alg-DA) conjugates and utilized polyvinyl alcohol (PVA) as the carrier polymer to fabricate a series of novel multifunctional composite nanofiber membranes (PVA/Alg-DA/CA) for promoting wound healing. These nanofiber membranes exhibited high water absorption, water vapor transmission rate, porosity, and hydrophilicity properties. The CA endowed the PVA/Alg-DA/CA membranes with excellent antibacterial properties, and the superior antioxidant activity to effectively protect cells from oxidative damage. Meanwhile, capitalizing on the unique nanofiber architecture, as well as the inherent biofunctional activities of CA and Alg-DA, these membranes exhibited remarkable biocompatibility, fostering a conducive environment for fibroblast adhesion and proliferation. Moreover, wound healing assessments and histopathological analyses revealed that composite membranes could promote neovascularization and tissue remodeling, and thus accelerating wound closure in the mouse full-thickness wound defect model. Additionally, the upregulation of key healing markers including CD31 and TGF- $\beta$ 1 protein expressions, further corroborated the ability of multifunctional membrane to stimulate the wound healing cascade. This multifunctional membranes with biosafety and therapeutic outcomes are a promising candidate for wound dressing to promote skin repair.

### 1. Introduction

Poor wound healing following trauma and surgical procedures represents a pressing global healthcare issue, affecting millions of individuals annually (Zhang, Huang, et al., 2024). The healing process for damaged skin tissue is highly complex, resulting from the concerted action of a series of cellular and molecular events (Qu et al., 2024). There is increasing evidence that reactive oxygen species (ROS) play a profound role in wound healing, which can control various processes such as inflammation, cell growth, angiogenesis, granulation tissue formation, and extracellular matrix deposition (Dong & Wang, 2023). However, an overabundance of ROS may cause cellular damage through membrane lipid peroxidation, sulfhydryl enzyme inactivation, protein cross-linking, and DNA decomposition (Liu et al., 2024). Particularly in

chronic wounds, the persistent inflammatory response leads to a significant accumulation of ROS, which will hinder the transition of the wound from the inflammatory phase to the proliferative phase, ultimately inducing delayed or failed wound healing (Zhang, Wu, et al., 2024). Therefore, enhancing effective local ROS management is crucial for the development of advanced wound dressings.

To date, a variety of modern wound dressings, such as nanofibers, sponges, foams, hydrogels, and others, have been developed to improve wound treatment and management (Wang, An, et al., 2024). Among them, electrospun nanofiber membranes have emerged as a promising option (Huang, An, et al., 2024). Nanofibers have been shown to enhance cell adhesion, and promote growth factor and collagen secretion by mimicking the extracellular matrix (ECM) (Prakashan et al., 2024). Furthermore, nanofiber membranes possess the capacity of

\* Corresponding authors.

E-mail addresses: zhengrunxiao@sdfmu.edu.cn (R. Zheng), jfqliu@sdfmu.edu.cn (J. Qiu), zhzhu@mail.ccnu.edu.cn (Z. Zhu).

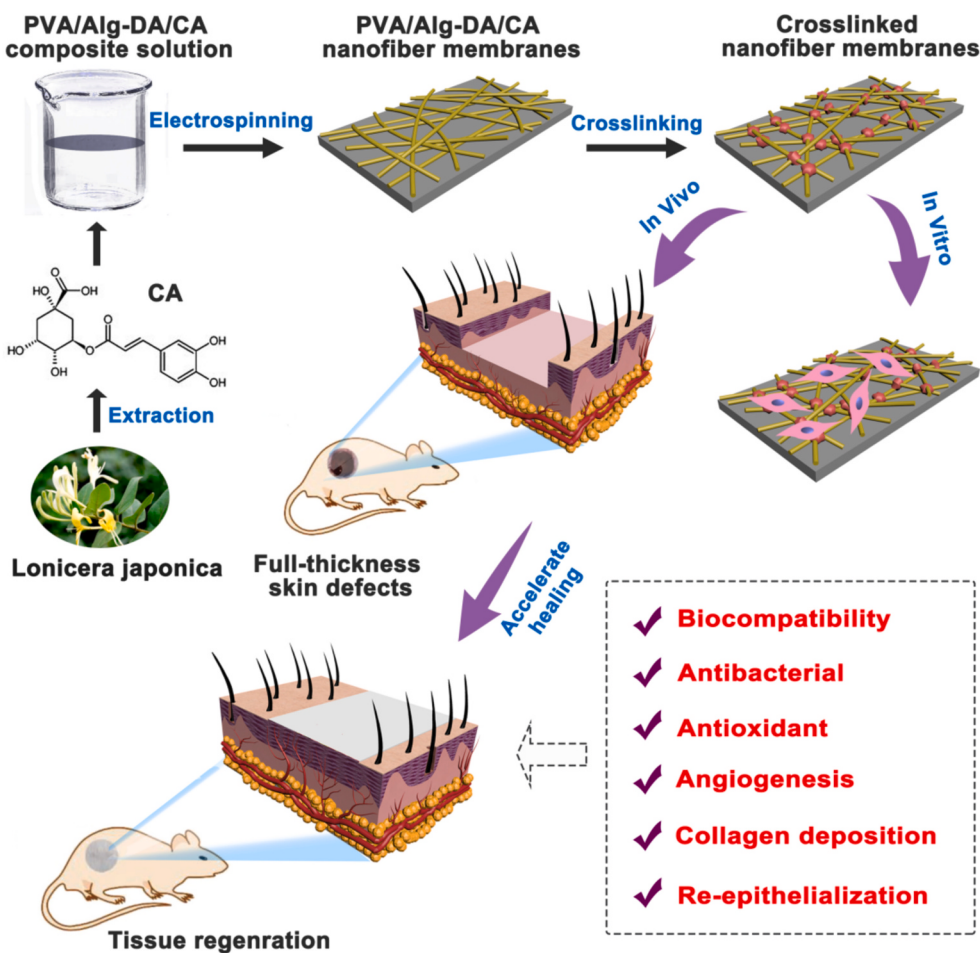


**Fig. 1.** Preparation and application of PVA/Alg-DA/CA composite nanofiber membranes in wound healing.

exudate absorption, moisture retention and adjustable morphology to achieve ideal characteristics conducive to wound closure (Song et al., 2024; Wang, Zhang, et al., 2024). In recent years, various reagents with antioxidant functions, such as thiol compounds, natural enzymes, and synthetic nanomaterials (e.g., CeO<sub>2</sub>, noble metal, etc.), have been introduced into nanofiber membranes to promote wound healing (Han et al., 2024; Zhou et al., 2023). However, all of them possess limitations and potential adverse effects. For instance, thiol compounds are susceptible to oxidation and may exhibit undesirable effects; while biological antioxidant enzymes can be expensive and prone to inactivation. Although antioxidant nanomaterials have showcased exceptional ROS scavenging capabilities and broad-spectrum elimination activities, their long-term *in vivo* safety and toxicity necessitate further rigorous investigation. Therefore, it is of paramount importance to explore safer and more effective antioxidants, and meanwhile, the design of wound dressings with multifunctional properties must also be considered.

Over the past few years, Chinese herbal medicines have received widespread attention owing to their availability and relatively low side effects. *Chlorogenic acid* (CA), the principal bioactive constituent of *Lonicerae japonica*, belongs to the class of natural polyphenol compounds renowned for their diverse biological activities. Extensive research has demonstrated its comprehensive biological attributes, including antioxidant, anti-inflammatory, anti-ulcerogenic, antitumor, and immunomodulatory properties (Song et al., 2024; Zhong et al., 2024). Recently, CA has also been shown to accelerate wound closure by promoting fibroblast proliferation and angiogenesis, as well as regulating macrophage polarization and epithelial formation during the wound healing process (Huang, Chen, Han, et al., 2023; Liu et al., 2024). Unfortunately,

the clinical application of CA is restricted by low bioavailability, stemming from its poor stability, rapid metabolism and elimination from the body. Despite the escalating interest in developing CA-loaded hydrogel systems for tissue engineering applications, the limitations of hydrogel wound dressings, including their inadequate exudate absorption and permeability, along with the intricate preparation process and potential toxicity of reagents, remain significant concerns. Given the inherent advantages of electrospun nanofibers, incorporating CA into a nanofiber-based wound dressing would be an effective strategy to augment wound healing outcomes.

Notably, biocompatibility and cell adhesion are another important feature required for wound dressings. Alginate (Alg) is a kind of natural linear anionic polysaccharide extracted from brown algae. It has excellent biocompatibility, rapid biodegradation, non-toxicity, and high protein absorption capacity, which is an ideal matrix of nanofiber dressing (Wang, Zhang, et al., 2024; Zhang, Yang, et al., 2024). However, although Alg-based nanofiber membranes can fill the tissue surrounding the fresh wound, absorb wound extract, and minimize bacterial infection, its inherent cell adhesion ability is limited stemming from the absence of dedicated cell adhesion sites (Suarez-Gonzalez et al., 2010; Zhang, Huang, et al., 2024). Dopamine (DA) has excellent wet adhesion to soft tissue attributed to chemical cross-linking and physical bonding between its catechol groups and soft tissue (Wang, Zhang, et al., 2024). Thus, modification of Alg with DA (alginate-dopamine conjugations (Alg-DA)) will endow Alg with good cell adhesion property. In addition, the biomaterials contained catechol groups have shown favorable antioxidant properties, which can expedite the wound repair process by balancing the oxidative stress (Ghorbani et al., 2024). Leveraging the unique functions of Alg, DA and bioactive CA, the

development of Alg-DA and CA-based composite nanofiber membranes to achieve multi-functional combined treatment is highly anticipated in wound healing, which has not been reported.

Due to the high conductivity, high surface tension and lack of chain entanglement caused by rigid and extended chain conformation of Alg in aqueous solution, it is challenges in directly fabricating Alg into nanofiber membranes (Wang, Ju, et al., 2020). PVA is a biodegradable water-soluble polymer with good fiber forming properties, high tensile strength, tensile modulus and wear resistance (Blanquer et al., 2024; Wang, Zhang, et al., 2024). Given its outstanding biocompatibility, PVA is an ideal candidate material for improving the electrospinning ability of Alg-based solutions. In this study, to enhance the electrospinnability and mechanical strength of Alg-DA, PVA was employed as a carrier polymer to fabricate a series of PVA/Alg-DA/CA composite nanofiber membranes through electrostatic spinning (Fig. 1). The good cytocompatibility and antibacterial properties of composite nanofiber membranes was systematically evaluated, while the underlying mechanisms of its antioxidant activity were also elucidated. Additionally, the wound healing potential of the functional membranes *in vivo* were assessed through wound closure analysis, histomorphological examination, and immunohistochemical staining. All of these results demonstrated this multifunctional nanofiber-based wound dressing is a promising candidate for the treatment and management of full-thickness diabetic wounds.

## 2. Materials and methods

### 2.1. Materials

Alginate (Alg, Chemically Pure, Viscosity:  $\geq 20$  (10 g/L, 20 °C)/mPa.s) was supplied by Sinopharm Chemical Reagent Co., Ltd. (Shanghai, China). Molecular weight = 2114 g/mol determined by gel permeation chromatography (GPC, PL-GPC 50), and the molecular weight distribution plot was shown in Fig. S1 (Huang, Chen, Hou, et al., 2023; Zhang et al., 2025). Mannuronate/Guluronate  $\approx 1$ , determined through Fourier transform infrared (FTIR) spectroscopy in Fig. S2 and Table S1 (Gómez-Ordóñez & Rupérez, 2011; Huang, Liao, et al., 2024; Sakugawa et al., 2004; Tordi et al., 2024). polyvinyl alcohol (PVA, Mw = 72,800–82,400 g/mol, 88 % hydrolyzed) was obtained from Shanghai Ying Jia Industrial Co., Ltd. Hydrochloric acid (HCl), glacial acetic acid, glutaraldehyde (GA, 25 %), FeSO<sub>4</sub>, hydrogen peroxide (H<sub>2</sub>O<sub>2</sub>, 30 %), absolute ethyl alcohol and salicylic acid were purchased from Sinopharm Chemical Reagent Co., Ltd. N-hydroxysuccinimide (NHS) and 1-ethyl-3-(3-dimethylaminopropyl) carbodiimide (EDC) were purchased from Shanghai Aladdin Co., Ltd. Dopamine hydrochloride and 1, 1-diphenylpicrylphenylhydrazine (DPPH) were supplied by Shanghai Maclin Biochemical Technology Co., Ltd. CA was obtained from Shanghai Bidd Pharmaceutical Technology Co., Ltd. Analytical grade materials and reagents were utilized in all experiments and used without any additional purification.

### 2.2. Preparation of Alg-DA conjugate

The synthesis of Alg-DA conjugate was performed following the method reported in the literature (Luo et al., 2019). Briefly, 1 g of Alg was dissolved in 100 mL of deionized water, and the solution pH was adjusted to between 4.5 and 5.5. After complete dissolution of Alg, 0.575 g of NHS and 0.959 g of EDC were sequentially added. The reaction mixture was stirred at room temperature for 45 min, followed by the addition of 0.948 g of DA. The mixture was then stirred overnight under a nitrogen atmosphere. Upon completion of the reaction, the resulting solution was purified by dialysis against deionized water for 3 days using a dialysis membrane. Subsequently, the purified product was freeze-dried and stored for future use.

### 2.3. Fabrication of nanofiber membranes containing Alg-DA conjugates

To overcome the challenges of electrospinning Alg/DA alone, PVA was used as an electrospinning aid to produce PVA/Alg-DA nanofibers. Specifically, PVA was employed as an electrospinning aid to fabricate PVA/Alg-DA nanofibers. Specifically, 750 mg of PVA were dissolved in 5 mL of deionized water and stirred at 80 °C until complete dissolved. Subsequently, 75 mg of Alg-DA was added to the above PVA solution to obtain PVA/Alg-DA solution. Actually, here the amount of Alg-DA added to the nanofibers represented the optimized effective ratio, which was the highest concentration achievable through electrospinning in our experiments. The electrospinning process was performed using commercial electrospinning equipment (ET-2535H, Beijing Ucalery Technology Development Co., Ltd., Beijing, China) Spinning parameters: the electric field strength was 16–17 kV, the distance between the nozzle and the receiver was 15 cm, the diameter of the spinneret needle was 20 G, the advancing rate was 0.04 mm/min, and the speed of the receiving device was 100 r/min. The nanofibrous membrane prepared by electrospinning was named as PVA/Alg-DA. Pure PVA nanofiber membranes were prepared by electrospinning the PVA solution without Alg-DA addition. Spinning parameters: the electric field strength was 12 kV, the distance between the nozzle and the receiver was 17 cm, the diameter of the spinneret needle was 20 G, the advancing rate was 0.16 mm/min, and the speed of the receiving device was 100 r/min. All nanofibrous membranes collected from aluminum foil were air-dried overnight.

### 2.4. Preparation of composite nanofiber membranes containing CA

After determining the optimal ratio of Alg-DA to PVA, varying masses of CA were added to 5 mL of the PVA/Alg-DA electrospinning solution, resulting in final CA concentrations of 0.5 mg/mL, 1 mg/mL, 2 mg/mL, 4 mg/mL, 8 mg/mL, and 16 mg/mL. The mixture was stirred at room temperature until complete dissolution. The prepared electrospinning precursor solution was then transferred into a syringe (5 mL) and mounted on a micro-syringe pump for electrospinning. The spinning parameters were set as follows: electric field strength of 16–17 kV, distance between the nozzle and collector of 15 cm, nozzle gauge of 20 G, feed rate of 0.02 mm/min, and receiver rotation speed of 100 r/min. After spinning, the nanofiber membranes were collected from the aluminum foil and dried overnight in air. The nanofiber membranes prepared with different CA concentrations were designated as PVA/Alg-DA/CA0.5, PVA/Alg-DA/CA1, PVA/Alg-DA/CA2, PVA/Alg-DA/CA4, PVA/Alg-DA/CA8, and PVA/Alg-DA/CA16, respectively.

### 2.5. Crosslinking of composite nanofiber membrane

The cross-linking process refers to the method reported in literature, and is slightly modified on this basis (Destaye et al., 2013). GA solution (25 %) was placed at the bottom of a drying tower, accompanied by glacial acetic acid solution as an acid catalyst. The PVA, PVA/Alg-DA, and PVA/Alg-DA/CA nanofiber membranes were then placed inside the drying tower and exposed to the vapor for 24 h. After completion of crosslinking, all fiber membranes were removed, dried in a vacuum oven for 48 h, and then stored in air for several weeks to remove residual glutaraldehyde and acetic acid solvents.

### 2.6. Materials characterization

The morphology and structure of the nanofiber films were observed by scanning electron microscopy (SEM, JSM-6700F, Japan). FTIR spectroscopy was performed using a Thermo Scientific Nicolet iN10 FTIR Microscope (Thermo Nicolet Corporation, USA) to confirm the chemical structures of Alg-DA conjugates and various nanofiber membranes. The surface wettability of each nanofiber membrane before and after crosslinking was measured using a Model 200 video-based optical

system (JC2000C1, Future Scientific Ltd. Co., China).

## 2.7. Water absorption capacity

The prepared nanocomposite membranes were cut into a 2 cm × 2 cm square and weighed ( $W_1$ ), then immersed in PBS buffer. After placed at 37 °C for 24 h, the membranes were taken out from the solution, and the superficial water was removed using a filter paper. The wet nanocomposite membranes were weighed ( $W$ ). The water absorption capacity was calculated according to the following formula:

$$\text{Water absorption (\%)} = \frac{W - W_1}{W_1} \times 100\%$$

where  $W_1$  and  $W$  are the dry weight and the wet weight of the nanocomposite membranes, respectively. The test was repeated three times.

## 2.8. Water vapor transmission rate

The Water vapor transmission rate (WVTR) of the nanocomposite membranes was evaluated according to the previously reported method (Ding et al., 2023). Specifically, 5 mL of PBS was added to the glass vial, then the mouth of the bottle was covered with nanofiber membranes and weighed ( $W_1$ ). After placed in a constant temperature oven at 37 °C for 24 h, the glass vial was weighed again ( $W_2$ ). The WVTR was calculated according to the following formula:

$$\text{WVTR (g/m}^2/\text{day}) = \frac{W_1 - W_2}{A}$$

where  $W_1$  and  $W_2$  are the initial and final weights, respectively, and  $A$  is the effective exposed area.

## 2.9. Porosity

With reference to the method reported in the literature (Ding et al., 2023), the porosity of nanofiber membranes were measured using the liquid displacement technique. Briefly, nanofiber membranes were prepared into rectangles and the volume was measured. Subsequently, these nanofiber membranes were soaked in anhydrous ethanol until saturated. The weight of membranes were measured before and after immersion in alcohol. The Porosity was calculated using the following formula:

$$\text{Porosity (\%)} = \frac{W_2 - W_1}{\rho \times V_1} \times 100\%$$

where  $W_1$  and  $W_2$  denote the weight of the membranes before and after immersion, respectively,  $V_1$  is the volume before immersion, and  $\rho$  is a constant of alcohol density.

## 2.10. In vitro release of CA

10 mg of PVA/Alg-DA/CA2, PVA/Alg-DA/CA4, PVA/Alg-DA/CA8 and PVA/Alg-DA/CA16 nanofiber membranes were weighed and immersed in 10 mL of PBS buffer, respectively, and incubated at 37 °C for 4 d. After a certain amount of time, remove 1 mL of solution and add the same volume of fresh PBS buffer. The absorbance of CA in the collecting medium was determined by ultraviolet-visible spectrophotometer (UV-vis, Lambda 750S, PerkinElmer, USA) at 325 nm. At the end of the release experiment, the CA retained in each nanofiber scaffold was extracted by ultrasonic extraction with ethanol as solvent, and the absorbance value of CA was measured. According to the pre-drawn standard curve of CA in PBS solution, the cumulative release amount of CA over time was calculated.

## 2.11. Antioxidant capacity of composite nanofiber membrane

First, the scavenging capacity of •OH was measured. The PVA/Alg-DA/CA1, PVA/Alg-DA/CA2, PVA/Alg-DA/CA4, PVA/Alg-DA/CA8 and PVA/Alg-DA/CA16 nanofiber membranes with a mass of 5 mg were immersed in 5 mL deionized water, respectively, and the sample solution was obtained by ultrasound for 30 min. 100 mL of 9 mM FeSO<sub>4</sub>, 9 mM salicylic acid-ethanol, and 8.8 mM H<sub>2</sub>O<sub>2</sub> solutions were precisely prepared for subsequent use. 1 mL of sample solution was weighed, then 1 mL of 9 mM FeSO<sub>4</sub> solution was added and mixed evenly. Then, 1 mL of 9 mM salicylic acid-ethanol solution was added. Finally, 1 mL of 8.8 mM H<sub>2</sub>O<sub>2</sub> solution was added to initiate the reaction. After 30 min of reaction at 37 °C, the absorbance of the mixed solution was measured at 510 nm wavelength with UV-vis and denoted as  $A_1$ . 1 mL deionized water was used instead of the sample solution as blank group, and the absorbance value was measured at 517 nm and denoted as  $A_0$ . With 1 mL deionized water instead of salicylic acid-ethanol solution as the control group, the spectrophotometric value measured at 517 nm was denoted as  $A_2$ . Hydroxyl radical clearance rate was calculated according to the following formula:

$$\text{Hydroxyl radical scavenging rate (\%)} = \left( 1 - \frac{A_1 - A_2}{A_0} \right) \times 100\%$$

Where  $A_0$  is the absorbance of blank control solution;  $A_1$  is the absorbance of the added sample;  $A_2$  is the absorbance of unadded salicylic acid-ethanol.

Next, the DPPH free radical scavenging ability was also performed. The PVA/Alg-DA/CA1, PVA/Alg-DA/CA2, PVA/Alg-DA/CA4, PVA/Alg-DA/CA8 and PVA/Alg-DA/CA16 nanofiber membranes with a mass of 5 mg were immersed in 5 mL of deionized water, respectively, and the sample solution was obtained by ultrasound for 30 min. Then 0.2 mM DPPH free radical ethanol solution was prepared, and 2 mL of the solution was added to the above 2 mL sample precursor solution. After the mixed solution was stirred in the dark for 30 min, the absorbance value of DPPH was measured at 517 nm wavelength by UV-vis and denoted as  $A_x$ . 2 mL of sample solution was added with 2 mL of deionized water, and the absorbance value was measured at 517 nm and denoted as  $A_{x0}$ . This group was used as the blank group. Instead of the sample solution, 2 mL of deionized water was added into 2 mL of 0.2 mM DPPH free radical ethanol solution. The absorbance value measured at 517 nm was denoted as  $A_0$ , and this group was used as the control group. DPPH clearance rate was calculated according to the following formula:

$$\text{DPPH free radical scavenging rate (\%)} = \left( 1 - \frac{A_x - A_{x0}}{A_0} \right) \times 100\%$$

Where  $A_0$  is the absorbance of DPPH radical and deionized water;  $A_x$  is the absorbance of each fiber membrane leaching solution and DPPH free radical;  $A_{x0}$  is the absorbance of each fiber membrane leaching solution and deionized water.

## 2.12. Cell viability assay

NIH-3T3 cells were cultured in DMEM medium supplemented with 10 vol% fetal bovine serum and 1 vol% penicillin/streptomycin. NIH-3T3 cells in the logarithmic growth phase were seeded into 96-well plates and cultured in a cell incubator at 37 °C with 5 % CO<sub>2</sub> for 24 h. Subsequently, the PVA, PVA/Alg-DA, PVA/Alg-DA/CA0.5, PVA/Alg-DA/CA1, PVA/Alg-DA/CA2, PVA/Alg-DA/CA4, PVA/Alg-DA/CA8, and PVA/Alg-DA/CA16 fiber membranes were gently transferred into each well. After co-incubation for 1, 3, and 5 d, the fiber membranes were removed, and the original medium was replaced with 200 µL of serum-free medium containing 10 % MTT reagent (Beyotime Biotechnology Co., Ltd., Shanghai, China), followed by continued incubation at 37 °C for 4 h. Subsequently, the MTT-containing medium was removed, and 150 µL of DMSO was added. After shaking for 10 min, the absorbance of

the solution was measured at 492 nm using a microplate reader (DNM-9602).

#### 2.13. Lactate dehydrogenase (LDH) activity assay

NIH-3T3 cells were seeded in 96-well plates and cultured for 24 h. Then the medium was replaced by fresh serum-free medium, and PVA, PVA/Alg-DA, PVA/Alg-DA/CA0.5, PVA/Alg-DA/CA1, PVA/Alg-DA/CA2, PVA/Alg-DA/CA4, PVA/Alg-DA/CA8 and PVA/Alg-DA/CA16 fiber membranes were gently transferred to each well. After 3 d of incubation, the culture medium from each well was collected into the centrifuge tube and centrifuged at 400 g for 5 min. Next, 120  $\mu$ L of the medium supernatants were put into a fresh 96-well plate and incubated with 60  $\mu$ L of LDH reagent (Beyotime Biotechnology Co., Ltd., Shanghai, China) for 30 min at 25 °C. The absorbance was measured using a microplate reader.

#### 2.14. Cell morphology observation

PVA, PVA/Alg-DA, PVA/Alg-DA/CA2, PVA/Alg-DA/CA4, and PVA/Alg-DA/CA8 membranes were placed at the bottom of 96-well plates, and NIH-3T3 cells were seeded onto the material surfaces. After co-incubated for 3 d, the cells were fixed with 3 % glutaraldehyde solution for 90 min, then dehydrated with a series of gradient ethanol solutions. After freeze-drying and gold spraying, cell morphology on the fiber membranes was observed by SEM. The morphology of NIH-3T3 cells cultured with different nanofiber matrices was also observed using a fluorescence microscope (NiKor-H550S, Japan). In brief, NIH-3T3 cells were inoculated in 24-well plates and incubated overnight. Then, fresh culture media containing composite fiber membranes were added and incubated for another 3 d. Afterwards, the cells were washed with PBS, and fixed with 3 % glutaraldehyde. After permeabilized with

0.5 % Triton X-100, the cell cytoskeleton and nuclei were stained with Phalloidin-Alexa Fluor-555 (Beyotime Biotechnology Co., Ltd., Shanghai, China) and 4, 6-diamidino-2-phenylindole (DAPI, Beyotime Biotechnology Co., Ltd., Shanghai, China) for 20 min, respectively, and observed by fluorescence microscopy.

#### 2.15. Establishment of NIH-3T3 cell oxidative damage model induced by $H_2O_2$

NIH-3T3 cells were seeded in a 96-well plate and cultured for 24 h. Then, the culture medium was discarded, and incomplete culture medium containing  $H_2O_2$  with final concentration of 0.2, 0.3, 0.4, 0.5, 0.6, 0.7, 0.8 and 0.9 mM was added. After 4 h of incubation, the  $H_2O_2$ -containing medium was discarded, and the cells were washed twice with PBS to remove  $H_2O_2$  residue. Next, 200  $\mu$ L of serum-free medium containing 10 % MTT reagent was added to each well. After incubation at 37 °C for 4 h, removing the supernatant and 150  $\mu$ L of DMSO was added. Following a 10 min shaking, the absorbance of the solution was measured at 492 nm using a microplate reader.

#### 2.16. Effect of composite nanofiber membrane on $H_2O_2$ -induced intracellular ROS level

NIH-3T3 cells were seeded into 24-well plates and cultured for 24 h. Then, PVA/Alg-DA/CA2, PVA/Alg-DA/CA4 and PVA/Alg-DA/CA8 fiber membranes were gently transferred to each well and cultured for another 24 h. Then, the old media and fiber membrane were discarded, and an appropriate concentration of  $H_2O_2$  was added to each well. After 4 h of incubation at 37 °C, the cells were washed with pre-cooled PBS, and exposed to DCFH-DA (Beyotime Biotechnology Co., Ltd., Shanghai, China) (10  $\mu$ M in serum-free medium), followed by additional incubation for 30 min at 37 °C. Finally, the intensity of intracellular green

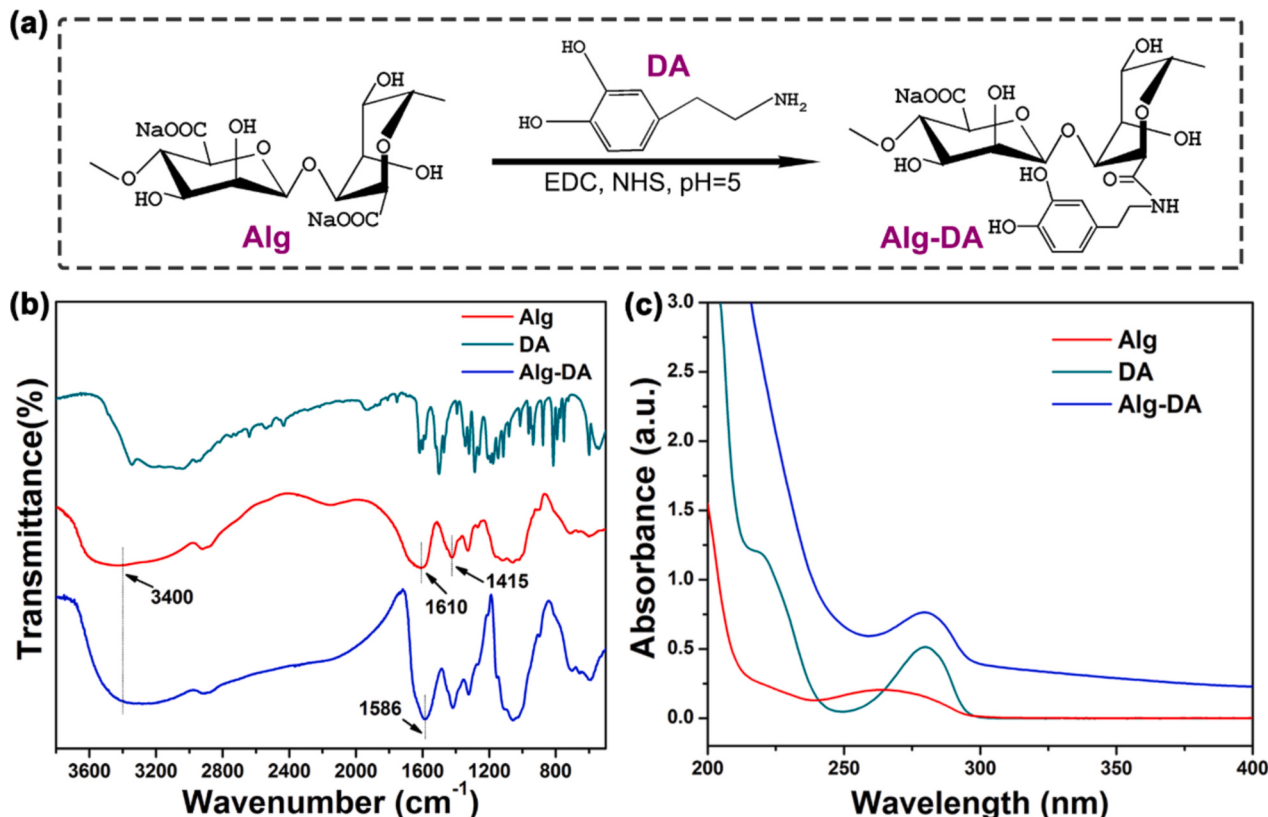


**Fig. 2.** (a) The schematic diagram of the synthesis of Alg-DA conjugates. (b) FTIR spectra of Alg, DA and Alg-DA conjugates. (c) UV-vis spectra of Alg, DA and Alg-DA conjugates.

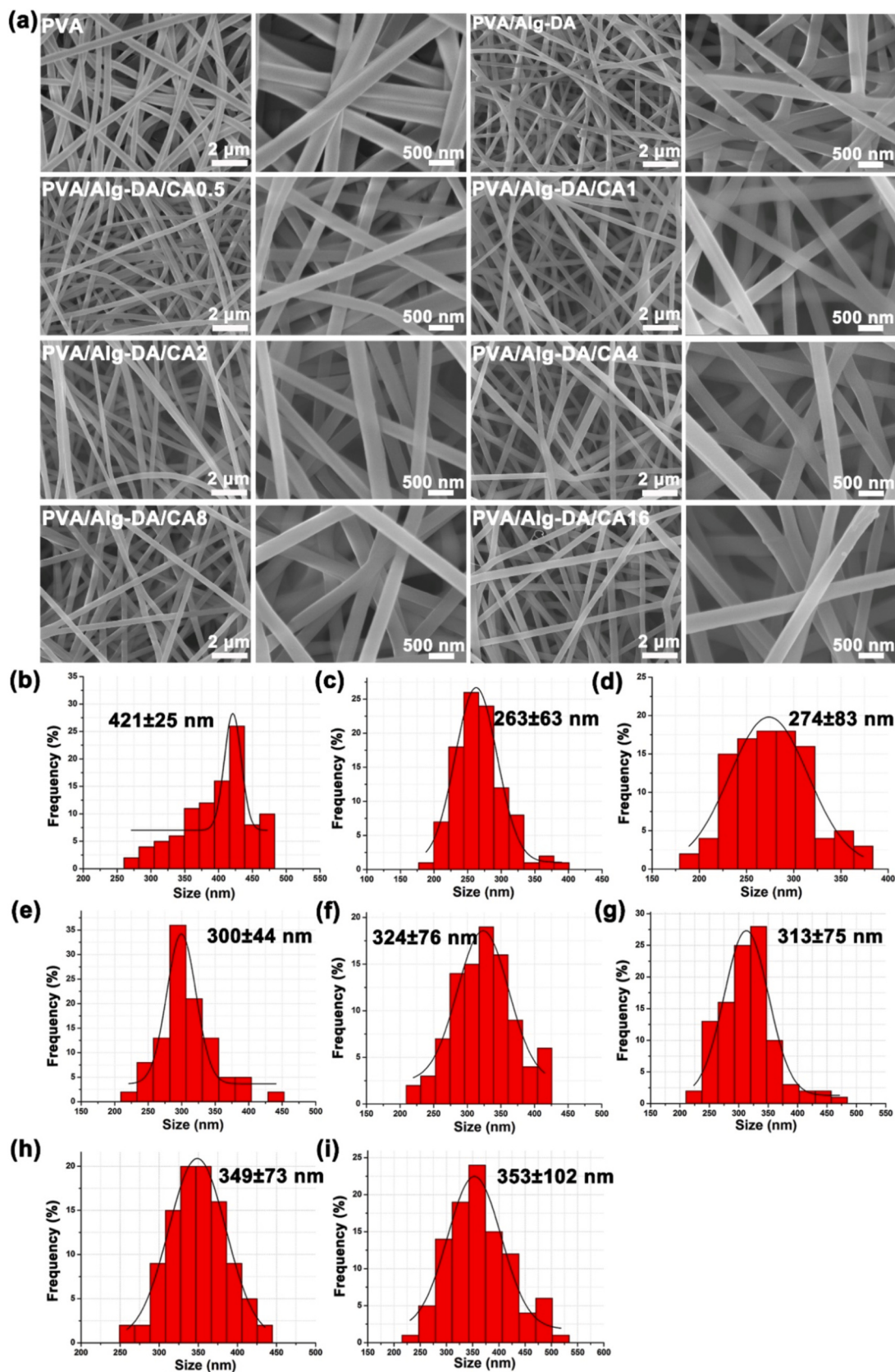


**Fig. 3.** (a) SEM images of nanocomposite membranes. (b-i) Diameter distribution of nanocomposite membranes.

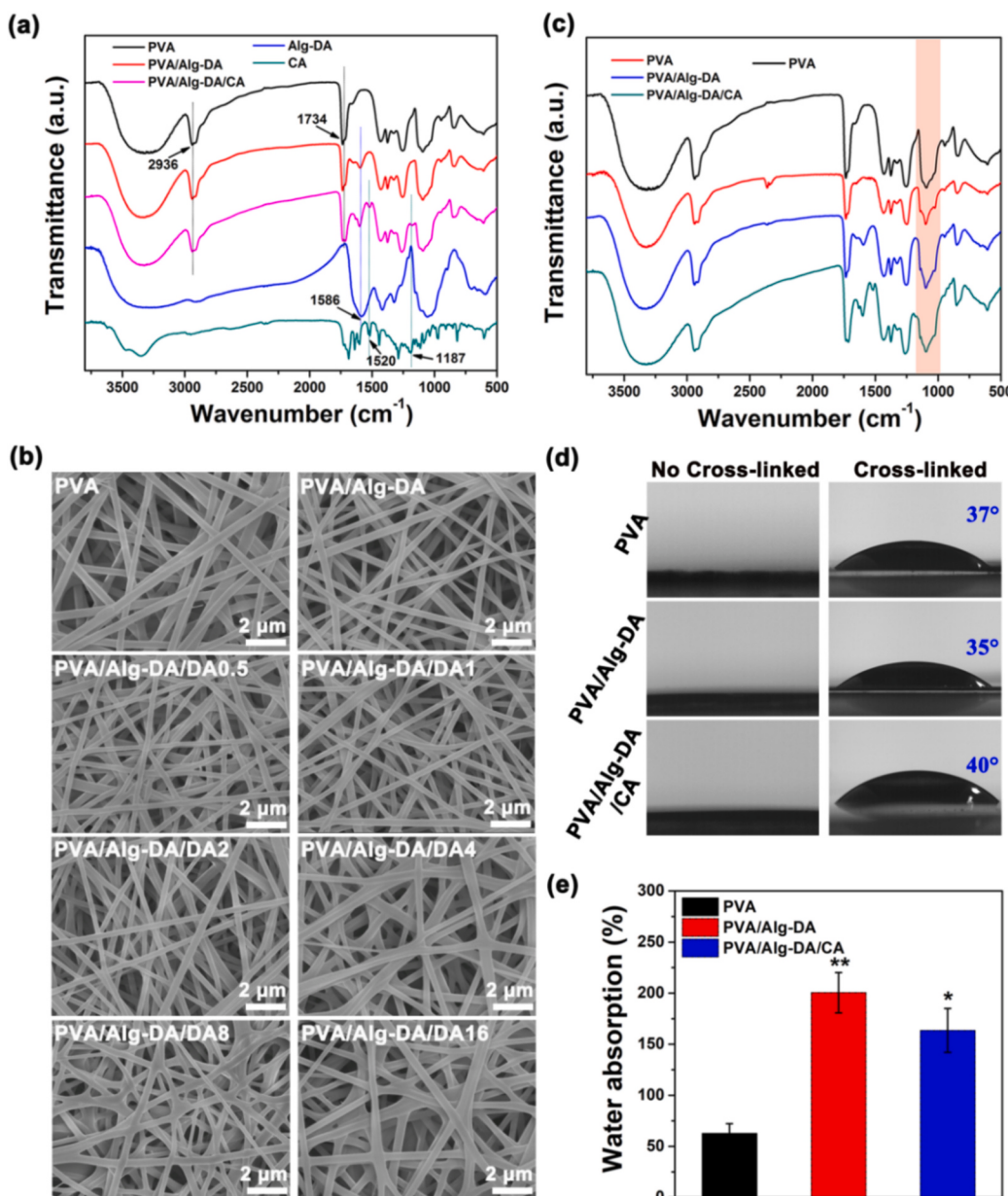


**Fig. 4.** (a) FTIR spectra of nanofiber membranes before crosslinking. (b) SEM images of cross-linked nanofiber membranes. (c) FTIR spectra of nanofiber membranes after crosslinking. (d) The contact angles of nanofiber membranes before and after crosslinking. (e) The water absorption rate of nanofiber membranes after crosslinking.

fluorescence was observed by fluorescence microscope.

#### 2.17. In vitro bacterial inhibition assay

To assess the antibacterial efficacy of the composite nanofiber membranes, gram-negative *Escherichia coli* (*E. coli*) (ATCC25922) and gram-positive *Staphylococcus aureus* (*S. aureus*) (ATCC29213) were used. Specifically, PVA, PVA/Alg-DA, PVA/Alg-DA/CA2, PVA/Alg-DA/CA4, and PVA/Alg-DA/CA8 fiber membranes were placed at the bottom of 24-well plates, and bacterial suspension with a concentration of  $1 \times 10^6$  colony-forming units· $\text{mL}^{-1}$  (CFU· $\text{mL}^{-1}$ ) were seeded onto the material surfaces. After bacteria colonization at 37 °C for 24 h, the bacterial suspension from each group was transferred into sterile tubes containing PBS solution and subjected to serial dilutions. Subsequently, 100  $\mu\text{L}$  of diluted suspension was spread on solid agar plates and incubated for another 18 h for CFU counting. Finally, the antibacterial rate was determined using the following formula:

$$\text{Antibacterial (\%)} = \frac{W - Q}{W} \times 100\%$$

where W is the number of colonies grown on agar plates after co-culture with PVA membranes and Q is the number of colonies grown on agar plates after co-culture with other nanocomposite membranes.

#### 2.18. In vivo wound healing assessment

Twenty 3-week-old male SD rats were purchased from SLAC Jingda Experimental Animal Co., LTD (Inspection Certificate NO. 430727201101530415). After one week of acclimatization, the rats were randomly divided into 5 groups (4 in each group), including blank control group, PVA/Alg-DA group, PVA/Alg-DA/CA2 group, PVA/Alg-DA/CA4 group and PVA/Alg-DA/CA8 group. The rats were anesthetized, their back hair was shaved and 70 % alcohol was disinfected to

create a round full-thickness skin wound with a diameter of 10 mm on their back. The wound in the control group was covered with gauze, and the wound in the experimental group was covered with PVA/Alg-DA, PVA/Alg-DA/CA2, PVA/Alg-DA/CA4 and PVA/Alg-DA/CA8 fiber membranes, respectively, and the whole wound was covered with a layer of medical tape to stabilize the dressing. The rats after modeling were raised in a single cage, and the day of modeling was recorded as day 0. The wounds were photographed with digital cameras at post-operative Days 0, 3, 7 and 14. On the 14th day after surgery, the rats were sacrificed, the whole skin tissue and adjacent skin tissue of the wound were cut, fixed with formaldehyde, embedded in paraffin, and sectioned. H&E and Masson staining were performed, respectively, and immunohistochemical (IHC) staining was performed for CD31 and TGF- $\beta$ 1 antibodies.

### 2.19. Statistical analysis

Each experiment in this study was repeated three times, and for the samples used in each experiment,  $n = 5$  or 6 were utilized. All data were analyzed using statistical software Origin 8.0 and presented as mean  $\pm$  standard deviation. The significance of differences between two groups was assessed using one-way ANOVA, followed by Student's *t*-test. Values of  $p < 0.05$  and  $p < 0.01$  were considered statistically significant and highly significant, respectively.

## 3. Results and discussion

### 3.1. Synthesis and characterization of Alg-DA conjugate

Alg lacks cellular adhesion sites, leading to generally poor cellular adhesion capacity. Inspired by Marine mussels, here Alg was modified with DA to endow Alg with outstanding cell adhesion and oxidation resistance. As shown in Fig. 2a, Alg was coupled with DA through classical EDC/NHS chemical reaction to synthesize Alg-DA coupling. In order to prevent DA oxidation and self-polymerization, the whole reaction process was carried out under the protection of  $N_2$  atmosphere. The chemical structures of the conjugated compounds were characterized by FTIR and UV-vis absorption spectra. As shown in Fig. 2b, in the spectrogram of Alg, the characteristic peak at  $3400\text{ cm}^{-1}$  was attributed to the stretching vibration of -OH group, while the characteristic peak at  $1610\text{ cm}^{-1}$  and  $1415\text{ cm}^{-1}$  corresponded to the symmetric and asymmetric stretching vibration of -COOH. Compared with the FTIR spectra of Alg and DA, the spectra of Alg-DA were similar to those of Alg, but the absorption peak of amide I bond appeared at  $1586\text{ cm}^{-1}$ , indicating that DA had been successfully grafted onto Alg. In addition, the Alg-DA sample showed a characteristic ultraviolet absorption peak of DA at  $280\text{ nm}$  (Fig. 2c), which further confirmed the successful coupling of DA and Alg.

### 3.2. Preparation and characterization of composite nanofiber membranes

Altering the polymer concentration could effectively modulate the fiber diameter and morphology. As shown in Fig. 3a, uniform nanofibers with an average diameter of  $421 \pm 25\text{ nm}$  were prepared using a 15 w/v % PVA solution. By optimizing various parameters, well-formed nanofibers with an average diameter of  $263 \pm 63\text{ nm}$  were produced at a PVA/Alg-DA mass ratio of 10/1. Furthermore, by varying the CA concentration, a series of composite nanofiber membranes with mesh-like porous structure, smooth surface, uniform size, and random orientation were prepared, with an average diameters (Fig. 3b-i) of  $274 \pm 83\text{ nm}$  (PVA/Alg-DA/CA0.5),  $300 \pm 44\text{ nm}$  (PVA/Alg-DA/CA1),  $324 \pm 76\text{ nm}$  (PVA/Alg-DA/CA2),  $313 \pm 75\text{ nm}$  (PVA/Alg-DA/CA4),  $349 \pm 73\text{ nm}$  (PVA/Alg-DA/CA8), and  $353 \pm 102\text{ nm}$  (PVA/Alg-DA/CA16), respectively. It has been demonstrated that electrospun nanofibers with homogeneous mesh-like porous structures and high specific surface area facilitate cell migration, adhesion, and differentiation on their surfaces

(Yang et al., 2022). Based on their structural advantages and the bioactive functionalities of CA and Alg-DA, the composite nanofibers would accelerate wound healing.

The chemical composition of various nanofiber membranes was further examined using FTIR spectroscopy. As depicted in Fig. 4a, in the PVA spectrum, the characteristic peak at  $2936\text{ cm}^{-1}$  was attributed to asymmetric stretching vibration of  $\text{CH}_2$ , while the absorption peak at  $1734\text{ cm}^{-1}$  was mainly related to the residual ester group  $\text{C=O}$  (Al Horani et al., 2024). All characteristic bands of PVA were included in the FTIR spectrum of PVA/Alg-DA; while the characteristic peak of Alg-DA appeared at  $1586\text{ cm}^{-1}$ , indicating that Alg-DA was evenly distributed in PVA/Alg-DA nanofibers. Similarly, in the spectra of PVA/Alg-DA/CA, the characteristic absorption peaks of PVA and Alg-DA appeared simultaneously, and two characteristic peaks of CA were detected at  $1520\text{ cm}^{-1}$  and  $1187\text{ cm}^{-1}$ . These signals confirmed the successful incorporation of both CA and Alg-DA into the nanofibers.

### 3.3. Characterization of crosslinked composite nanofiber membrane

Due to the water-soluble nature of PVA, Alg, and DA, the obtained electrospun PVA/Alg-DA/CA nanofiber membranes instantly dissolved upon immersion in water, limiting their potential biomedical application. To increase the water-resistant ability of the nanofiber membranes, the electrospun PVA/Alg-DA/CA membranes were modified using GA vapor-phase crosslinking. The PVA, PVA/Alg-DA, and PVA/Alg-DA/CA membranes were exposed to a closed container containing GA vapor, with glacial acetic acid solution placed as an acid catalyst. As shown in Fig. 4b, after the cross-linking reaction, the originally straight nanofibers were fused and intertwined, forming fusions at their intersection points. This was likely due to the softening and swelling of the nanofiber surfaces caused by water vapor from the GA solution, facilitating inter-fiber adhesion (Kumar et al., 2019). Furthermore, the hydroxyl groups of the PVA nanofibers interacted with the aldehyde ends of GA, forming acetal bridges at the contact points between these fibers (Destaye et al., 2013). To confirm this view, FTIR spectra of the cross-linked nanofibers were characterized. As shown in Fig. 4c, compared with those of the nanofibers without cross-linked, in the FTIR spectra of cross-linked PVA, PVA/Alg-DA and PVA/Alg-DA/CA nanofiber membranes, the vibration band broadening of aldehyde group O-C-O was observed at  $1000\text{--}1140\text{ cm}^{-1}$ . This indicated the successful cross-linking between PVA and aldehyde ends of GA.

In order to test the wettability of the nanofiber membranes after cross-linking, the water contact angles of PVA, PVA/Alg-DA and PVA/Alg-DA/CA nanofiber membranes before and after cross-linking were measured. As shown in Fig. 4d, before cross-linking, water droplets on all nanofiber membranes were completely spread and absorbed, resulting in a contact angle of  $0^\circ$ , indicating the superhydrophilicity of membranes. However, after crosslinking modification, the contact angles of PVA, PVA/Alg-DA, and PVA/Alg-DA/CA membranes increased to  $37^\circ$ ,  $35^\circ$ , and  $40^\circ$ , respectively, suggesting a decrease in hydrophilicity. These results demonstrated that GA vapor-phase crosslinking successfully improved the surface wettability of the composite membranes. Surface wettability is categorized based on the contact angle ( $\theta$ ) as follows: superhydrophilic ( $\theta < 25^\circ$ ), highly hydrophilic ( $25^\circ < \theta < 90^\circ$ ), low hydrophilic ( $90^\circ < \theta < 150^\circ$ ), and superhydrophobic ( $\theta > 150^\circ$ ) (Ahn et al., 2019). Studies have indicated that hydrophilic nanofibers significantly affect the initial adhesion and proliferation of cells and create an optimal environment for the release of bioactive molecules (Nematollahi et al., 2025). Additionally, here the crosslinked PVA/Alg-DA/CA nanofiber membranes with a highly hydrophilic surface would also allow for quick absorption of wound blood and exudate, and promoting hemostasis.

The ability to absorb wound exudate well is one of the important indicators of a good wound dressing (Sadeghi-Aghdash et al., 2024). To confirm the ability of composite membranes to absorb wound exudate, the water absorption test was performed. As shown in Fig. 4e, the water

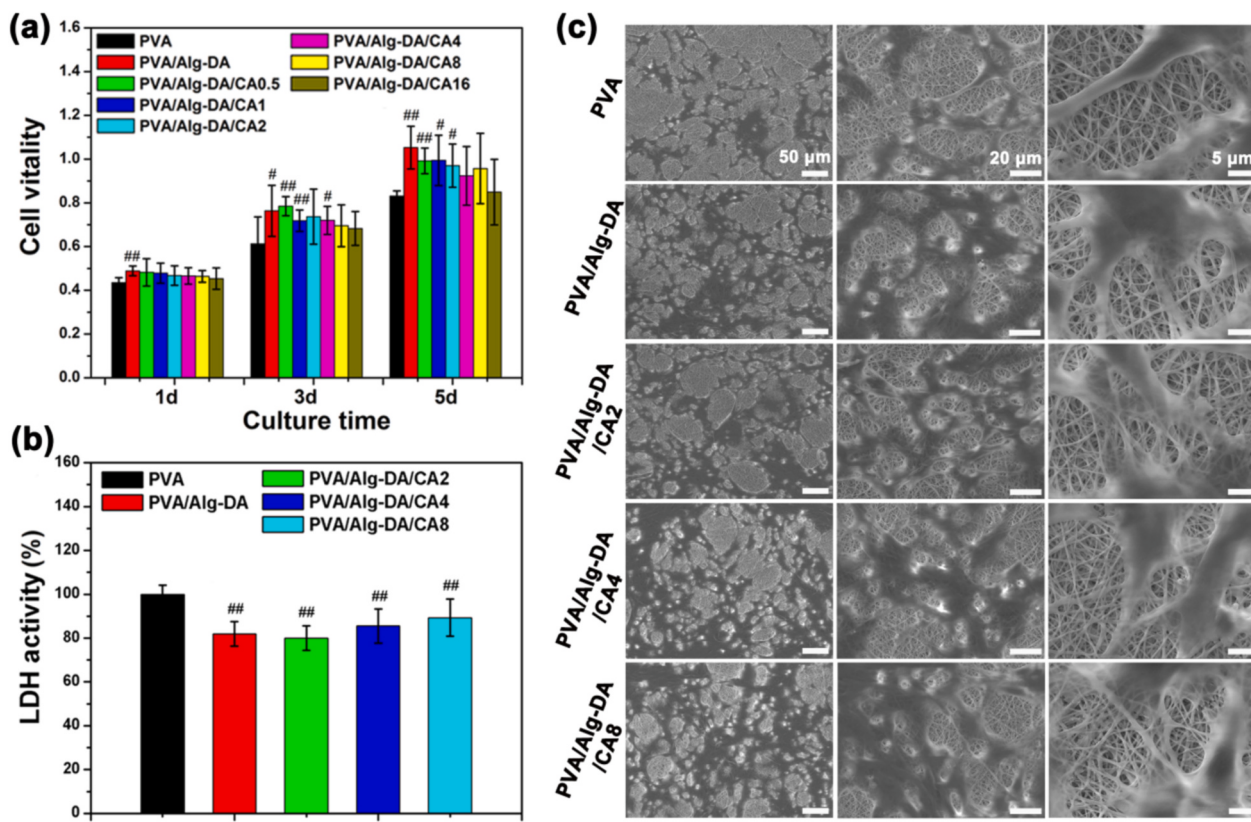


**Fig. 5.** (a) Cell viability of NIH-3T3 cells cultured with different nanofiber membranes for 1, 3 and 5 days. (b) LDH activity in culture medium after NIH-3T3 cells were cultured with different nanofiber membranes for 3 days. #P < 0.05 and ##P < 0.01 compared with PVA. (c) SEM images of NIH-3T3 cells after seeding on different nanofiber membranes for 3 days.

absorption of PVA, PVA/Alg-DA, and PVA/Alg-DA/CA membranes reached  $62.68 \pm 9.52\%$ ,  $200.44 \pm 19.74\%$  and  $163.52 \pm 21.54\%$  of their initial weight after 24 h, respectively. The water absorption of PVA/Alg-DA and PVA/Alg-DA/CA was significantly higher than that of PVA, which could be attributed to the addition of Alg-DA. The presence of hydrophilic functional groups, such as carboxyl and amino groups in nanofibers, have been verified to improve the water absorption capacity of the membranes (Doostan et al., 2023). The good water uptake ability of the prepared composite membranes was conducive to accelerate wound healing process by absorbing wound effluence and reducing the probability of infection.

Water permeability of polymeric wound dressings is also important for biomedical applications. Here, the water permeability behavior of composite membranes was measured by WVTR test. As shown in Fig. S3, the WVTR was  $826.85 \pm 24.95 \text{ g/m}^2/\text{day}$  for the PVA,  $1013.77 \pm 29.68 \text{ g/m}^2/\text{day}$  for the PVA/Alg- DA, and  $984.30 \pm 33.15 \text{ g/m}^2/\text{day}$  for the PVA/Alg-DA/CA. Previous research reported that water permeability was directly influenced by the porosity of nanofiber mats caused by fiber diameter (Ding et al., 2023). The WVTR of PVA/Alg-DA and PVA/Alg-DA/CA were significantly higher than that of PVA could be attributed to the possible expanded pore size of the composite membranes and after the addition of Alg-DA. It has been indicated that effective wound dressings typically have a WVTR between 904 and 1447  $\text{g/m}^2/\text{day}$  (Ding et al., 2023). The prepared PVA/Alg-DA/CA nanofiber membranes fell within this desirable range, which would provide a proper gas exchange for wound healing and reduce wound infection or scar formation.

High porosity aids in the exchange of oxygen and essential nutrients required for wound healing, while also offering sufficient space for cellular growth and migration (Sun et al., 2022). Therefore, the porosity of composite membranes were further measured. The results in Fig. S4 exhibited that the porosity of PVA was  $65.95 \pm 4.72\%$ . Compared to

PVA, the addition of Alg-DA significantly improved the pore size of PVA/Alg-DA and PVA/Alg-DA/CA membranes, which increased to  $82.51 \pm 3.48\%$  and  $80.91 \pm 3.01\%$ , respectively. The high porosity indicated the effectiveness of PVA/Alg-DA/CA nanofiber membranes as wound dressings.

#### 3.4. Release of CA in vitro

Using PVA/Alg-DA/CA2, PVA/Alg-DA/CA4, PVA/Alg-DA/CA8, and PVA/Alg-DA/CA16 fiber membranes as representatives, the *in vitro* release behavior of CA from different drug-loaded fiber membranes was investigated using PBS as the release medium. Fig. S5a showed the standard curve of CA at 325 nm, and Fig. S5b showed the cumulative release rate (%) of CA at different time points. As can be seen from the figures, the cumulative release rate of CA increased gradually with the increase of CA concentration in the fiber membrane. On day 4, 60 %, 66 %, 74 % and 81 % of CA were released from the PVA/Alg-DA/CA2, PVA/Alg-DA/CA4, PVA/Alg-DA/CA8 and PVA/Alg-DA/CA16 membranes, respectively. The release profiles of all composite membranes were found to be generally similar throughout the experimental period, exhibiting an initial burst release behavior within the first 12 h, followed by a gradual slowdown in the release rate. Both drug diffusion and polymer degradation contributed to the overall drug release. The initial burst release was primarily attributed to the rapid release of CA present on the fiber surface. The subsequent sustained release mechanism might be due to enhanced interactions between CA molecules and Alg-DA, which hindered drug diffusion. The incorporation of active molecules or drugs in nanofiber membranes has been one of the effective strategies to address the rapid release of drugs (Jiang et al., 2023). The results of *in vitro* drug release confirmed that PVA/Alg-DA/CA had a sustained release behavior, which could enhance the permeability of CA at the

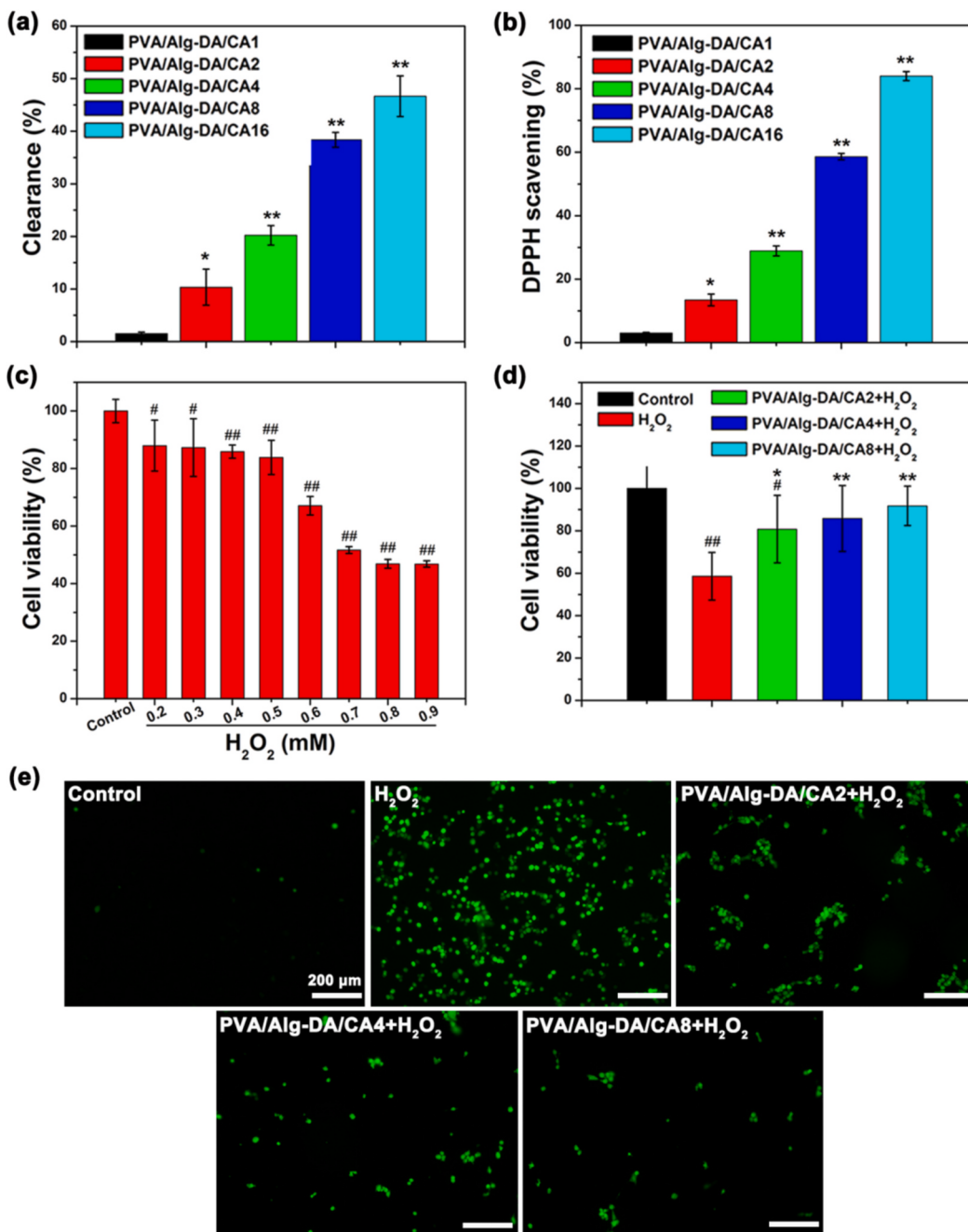


**Fig. 6.** (a) Hydroxyl radical scavenging rate of composite nanofiber membranes. (b) DPPH clearance rate of composite nanofiber membranes. \* $P < 0.05$  and \*\* $P < 0.01$  compared with PVA/Alg-DA/CA1. (c) Cell viability of NIH-3T3 cells cultured with different concentrations of H<sub>2</sub>O<sub>2</sub>. # $P < 0.05$  and ## $P < 0.01$  compared with control. (d) The effect of composite nanofiber membranes on the cell vitality of NIH-3T3 cells induced by H<sub>2</sub>O<sub>2</sub>-induced oxidative damage. # $P < 0.05$  and ## $P < 0.01$  compared with control, \* $P < 0.05$  and \*\* $P < 0.01$  compared with H<sub>2</sub>O<sub>2</sub> group. (e) Detection of intracellular ROS levels in NIH-3T3 cells by DCFH-DA (a ROS fluorescent probe, green).

wound site and thus improved its bioavailability.

### 3.5. Biocompatibility of composite nanofiber membrane

Wound dressings directly interact with damaged skin, biocompatibility is a prerequisite for effective wound management. During wound healing, fibroblasts play a vital role in the formation of granulation tissue and new collagen structures during wound healing (Wang et al., 2025). In this study, the biocompatibility of the composite membranes was assessed by MTT assay, LDH test and cell morphology observation using NIH-3T3 cells as a model system. As shown in Fig. 5a, NIH-3T3 cells were co-cultured with PVA, PVA/Alg-DA, and PVA/Alg-DA/CA

composite nanofibrous membranes containing varying concentrations of CA, and the cell viability and proliferation were analyzed. All groups exhibited a significant proliferation trend within 5 d, indicating healthy cell growth throughout the experimental period. On day 1, except for the PVA/Alg-DA group, there were no notable differences in cell activity compared to the PVA group. After 3 and 5 d of co-incubation, the cell numbers in all other groups increased significantly compared to the PVA group. On day 3, the PVA/Alg-DA, PVA/Alg-DA/CA0.5, PVA/Alg-DA/CA1, and PVA/Alg-DA/CA4 groups displayed significantly higher cell activity than the PVA group. By day 5, the PVA/Alg-DA, PVA/Alg-DA/CA0.5, PVA/Alg-DA/CA1, and PVA/Alg-DA/CA2 groups showed marked differences in cell activity compared to the PVA group.

However, it was noteworthy that as the CA content increased in the PVA/Alg-DA/CA membranes, a general trend of decreased cell activity was observed compared to PVA/Alg-DA. This results suggested that within a certain concentration range, CA had no adverse effects on NIH-3T3 cells but might inhibit cell growth at higher concentrations. Based on the MTT results and concerns about potential adverse effects of high CA concentrations on cells, we selected PVA/Alg-DA/CA8 nanofibrous membranes as the highest CA concentration group for subsequent experiments and utilized PVA/Alg-DA/CA2 and PVA/Alg-DA/CA4 nanofibrous membranes as comparators.

Typically, membrane damage caused by apoptosis or necrosis of cells induces the release of LDH from the cytoplasm into the culture medium (Zhang et al., 2022). Consequently, the amount of released LDH correlates with cytotoxicity. After co-culturing NIH-3T3 cells with different nanofiber membranes for 3 d, the LDH activity in the culture medium was analyzed. The results in Fig. 5b showed that the LDH activity matching with the PVA/Alg-DA and PVA/Alg-DA/CA groups were significantly lower than that corresponding to PVA group. This indicated that CA-loaded nanofiber membranes had no adverse effect on normal cell growth.

Cell morphology is an important index to evaluate the safety of biomaterials (Nezari et al., 2023). Therefore, the adhesive morphologies of NIH-3T3 cells cultured on different membranes were further observed by SEM. As depicted in Fig. 5c, after 3 d of culture, NIH-3T3 cells seeded on different fibrous membranes exhibited robust cell adhesion. Cells on the PVA membrane displayed an active polygonal morphology with well-stretched cellular extensions and protruding lamellipodia, indicating that the nanofiber surface favored cellular spreading and growth. In comparison to the PVA group, a notably higher number of cells adhered to the PVA/Alg-DA fibrous membrane, with tightly bound attachment between adjacent cells and more extensive extensions of filopodia and lamellipodia. Furthermore, we observed similar growth trends of NIH-3T3 cells on various PVA/Alg-DA/CA fibrous membranes, characterized by abundant filopodia, tighter intercellular connections, and increased cell numbers. These results collectively demonstrated that PVA/Alg-DA/CA nanofibers possessed excellent bioactivity, which was beneficial to the adhesion, spreading, and proliferation of fibroblasts. In order to evaluate the effect of the composite membrane on the surrounding cells, we further analyzed the morphological changes of NIH-3T3 cells after incubation with various nanofiber membranes for 3 d by fluorescence microscopy. As can be seen from Fig. S6, cells in all groups exhibited complete spreading, well-developed cytoskeletons, and well-stretched actin bundles. It was worth mentioning that compared with the PVA group, cells cultured with PVA/Alg-DA/CA and PVA/Alg-DA nanofiber membranes showed significantly increased cell density and higher cell aggregation.

Together, these results confirmed the excellent biocompatibility of these composite nanofiber membranes, as evidenced by enhanced attachment, spreading and proliferation of NIH-3T3 cells. The good biocompatibility of PVA/Alg-DA/CA was attributed to the synergistic effect of the ECM-mimicking structure of nanofibers and the presence of multiple active substances in the membranes. Recent research have elucidated the roles of nanofiber structure in affecting gene expression of laden cells related to cytoskeleton, promotion of cell cycle progression, cell adhesion, and cell proliferation (Wang, Meng, et al., 2023). Meanwhile, the favorable effect of Alg on cell growth has long been confirmed (De Silva et al., 2018). In addition, the catechol groups on DA have adhesion and antioxidant properties, allowing potential attachment at the site of injury and better synergies with other substances (Fadilah et al., 2023). Our results revealed that CA had a dose-dependent effect on cell growth, while the released CA from the composite membranes could be safe. Taken together, these results demonstrated the promising biological safety of PVA/Alg-DA/CA membranes and potential as wound dressing.

### 3.6. Antioxidant capacity and protective effect of composite nanofiber membrane on $H_2O_2$ -induced oxidative damage of NIH-3T3 cells

Excessive production of free radicals at the wound site can induce oxidative stress, leading to lipid peroxidation, DNA damage, and enzyme inactivation, thereby delaying wound healing (Hunt et al., 2024). The local application of biomaterials with free radical scavenging properties can significantly improve wound healing in patients or animals (Fadilah et al., 2023). Consequently, here we first evaluated the *in vitro* antioxidant activity of PVA/Alg-DA/CA fiber membranes through their scavenging abilities against •OH and DPPH free radicals, with the scavenging rates quantified as the percentage inhibition of free radical formation. As depicted in Fig. 6a, the scavenging capability of the composite nanofibrous membranes gradually increased with the increase in CA concentration in the •OH scavenging assay. Similarly, the DPPH scavenging rate also significantly increased with the rise in CA concentration (Fig. 6b). Notably, the PVA/Alg-DA/CA16 fibrous membrane exhibited the strongest antioxidant activity, with scavenging rates of 46.7 % and 84.0 % against •OH and DPPH free radicals, respectively. These results indicated that the incorporation of CA effectively enhanced the antioxidant activity of the composite nanofibrous membranes. In addition, the catechol groups contained in DA also endowed certain antioxidant properties on nanofiber membranes, which have been confirmed by previous studies (Wang, Zhao, et al., 2023). It has reported that CA acts as a free radical scavenger and exerts its antioxidant activity primarily due to its abundant phenolic hydroxyl functional groups (Rojas-Gonzalez et al., 2022). Higher concentrations of CA released from PVA/Alg-DA/CA fibrous membranes with high CA content dissolve in the solution, thereby demonstrating stronger scavenging rates against •OH and DPPH free radicals. In conclusion, the excellent antioxidant capability of PVA/Alg-DA/CA augmented its potential application in skin wound dressings.

To evaluate the intracellular ROS scavenging capability of the composite nanofiber membranes, we initially established an  $H_2O_2$ -induced oxidative stress model in NIH-3T3 cells.  $H_2O_2$ , a commonly used oxygen radical generator in cells, can penetrate cell membranes and react with various intracellular enzymes to generate highly reactive free radicals, ultimately leading to cell or tissue damage (Wang et al., 2016). NIH-3T3 cells were exposed to varying concentrations of  $H_2O_2$  for 4 h, and cell viability was determined using the MTT assay. As shown in Fig. 6c, the effect of  $H_2O_2$  on cell viability displayed a concentration-dependent relationship within the range of 0.2–0.9 mM. With increasing  $H_2O_2$  concentrations, the inhibitory effect on cells was intensified, indicating a gradual aggravation of oxidative damage. Notably, when NIH-3T3 cells were treated with a final concentration of 0.7 mM  $H_2O_2$ , cell viability significantly decreased to 51.7 %, approaching the half-maximal inhibitory concentration ( $IC_{50}$ ). Consequently, this concentration was selected as the optimal concentration for inducing the damage model.

Subsequently, to investigate the protective effects of the composite membranes against  $H_2O_2$ -induced oxidative damage in NIH-3T3 cells, oxidative damaged NIH-3T3 cells were treated with PVA/Alg-DA/CA2, PVA/Alg-DA/CA4, and PVA/Alg-DA/CA8 membranes, and cell viability was assessed. As shown in Fig. 6d, upon exposure to 0.7 mM  $H_2O_2$ , the cell viability decreased to approximately 58.5 % of the control group. However, when NIH 3T3 cells were pre-treated with PVA/Alg-DA/CA membranes for 24 h and then exposed to  $H_2O_2$ , the cell viability was significantly improved compared to the cells exposed only  $H_2O_2$ . Specifically, cell viability increased to 80.8 %, 85.8 %, and 91.7 % with the addition of PVA/Alg-DA/CA2, PVA/Alg-DA/CA4, and PVA/Alg-DA/CA8 composite nanofibrous membranes, respectively, showing concentration-dependent tolerance to CA. This finding indicated that PVA/Alg-DA/CA composite membranes exhibited significant protective effects against  $H_2O_2$ -induced cell damage, with the bioactive molecule CA playing a pivotal role. To validate this, we further explored the ROS-scavenging capacity of the composite membranes in  $H_2O_2$ -induced

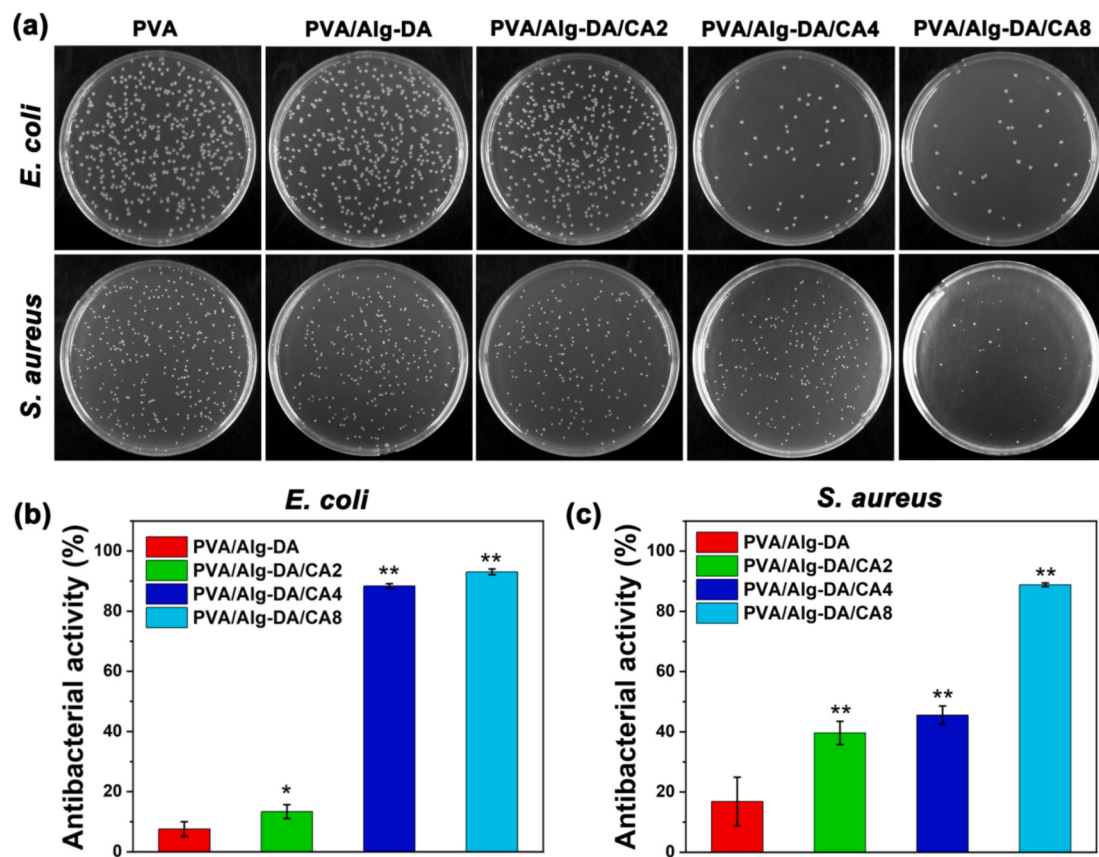


**Fig. 7.** (a) The inhibition ability of nanocomposite membranes on *E. coli* and *S. aureus*. (b) Quantitative analysis of anti-*E. coli* of nanocomposite membranes. (c) Quantitative analysis of anti-*S. aureus* of nanocomposite membranes. \* $P < 0.05$  and \*\* $P < 0.01$  compared with PVA/Alg-DA.

oxidative cells using DCFH-DA as a fluorescent probe. DCFH-DA is used as an indicator for ROS because it can be oxidized by peroxy radicals to generate strong green fluorescent 2,7-dichlorofluorescein (Zhang et al., 2023). Therefore, the inhibition effect of PVA/Alg-DA/CA membranes on H<sub>2</sub>O<sub>2</sub>-induced ROS could be directly evaluated by intracellular fluorescence intensity. As can be seen from Fig. 6e, under a fluorescence microscope, strong green fluorescence was observed in the H<sub>2</sub>O<sub>2</sub>-treated group, indicating a high level of intracellular ROS. Interestingly, compared to the damaged group (H<sub>2</sub>O<sub>2</sub> group), all PVA/Alg-DA/CA-treated groups exhibited significantly reduced ROS levels, with fluorescence intensity gradually decreasing with increasing CA doses. These results confirmed that the incorporation of CA into the composite membranes effectively inhibited the generation of intracellular ROS.

A large number of studies have proved that the presence of excess ROS is a major obstacle to wound healing, which can degrade extracellular matrix proteases and damage fibroblasts, resulting in impaired angiogenesis and slow tissue regeneration (Hunt et al., 2024). Therefore, the PVA/Alg-DA/CA nanofiber membranes were able to protect the cell against cytotoxicity generated by H<sub>2</sub>O<sub>2</sub>, which might be attributed to its antioxidant ability to scavenge intracellular ROS. As a natural phenolic compound, CA has been reported to scavenge free radicals and resist lipid peroxidation in different organs (Shah et al., 2021; Zhang, Wu, et al., 2024). In addition, the antioxidant properties mediated by phenolic groups contained in DA have also been proved to be effective in protecting cells from damage caused by oxidative stress and supporting normal cellular life activities (Liu et al., 2024). As a result, the composite membranes we developed acting as an excellent ROS scavenger would contribute to rapid wound healing under oxidative stress condition.

### 3.7. Antimicrobial effect of composite nanofiber membrane

Bacterial infections can generate ROS and hinders wound healing, so the development of wound healing dressings with antimicrobial properties is of great significance in clinical applications (Chai et al., 2023). In this work, the *in vitro* antibacterial properties of composite membranes against Gram-negative *E. coli* and Gram-positive *S. aureus* were investigated using the spread plate method. As shown in Fig. 7a, many colonies of *E. coli* and *S. aureus* were observed in the PVA and PVA/Alg-DA groups, while the amount of visible bacterial colonies in PVA/Alg-DA/CA groups continued to decrease with the increasing concentrations of CA. The results in Fig. 7b showed that PVA/Alg-DA had an antibacterial rate of 7.56 ± 2.42 %, and the antibacterial rate for PVA/Alg-DA/CA2, PVA/Alg-DA/CA4, and PVA/Alg-DA/CA8 groups reached to 13.35 ± 2.29 %, 88.38 ± 0.74 %, and 93.08 ± 0.98 %, respectively. The antibacterial rate of PVA/Alg-DA/CA groups was significantly higher than that of PVA group. Similarly, the antibacterial effects for *S. aureus* (Fig. 7c) observed in PVA/Alg-DA/CA2, PVA/Alg-DA/CA4, and PVA/Alg-DA/CA8 groups were contingent upon the concentration of CA, with the PVA/Alg-DA/CA8 group exhibiting the most pronounced antibacterial effect. It was found that the inhibition rates against *S. aureus* in the PVA/Alg-DA/CA8 group was 88.83 ± 0.62 %. Overall, these results confirmed the outstanding *in vitro* antibacterial ability of PVA/Alg-DA/CA composite membranes.

The antibacterial actions of PVA/Alg-DA/CA could be attributed to the porous structure of the nanofiber surface increased the adhesion sites for bacteria (Li et al., 2025). Besides, the membranes continuously released CA, which interacted strongly with bacterial cell membranes, disrupting bacterial cell wall and impairing the cell integrity (Wang, Zhai, et al., 2020). Studies have shown that severe rupture of the bacterial membrane can lead to the leakage of DNA and RNA, which

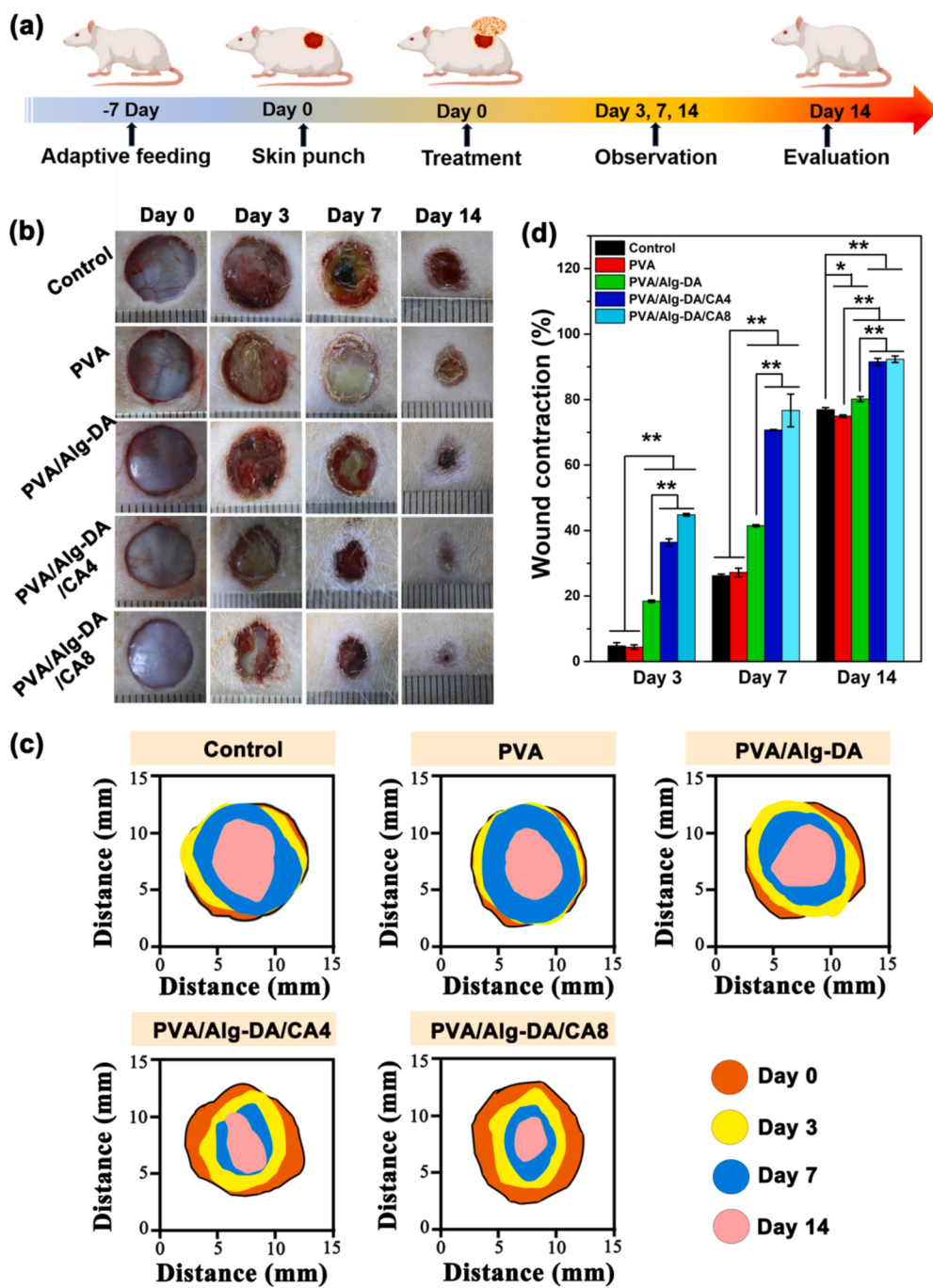


**Fig. 8.** (a) Schematic illustration of the timeline of animal experiments to test the therapeutic effect of nanofiber membrane. (b) Representative photographs of the wounds in different treatment groups at different time points. (c) Evidence of wound-bed closure over the course of 14 days in each group. (d) Quantification of wound healing area at various healing periods in each group.

ultimately resulting in bacteria death (Seaberg et al., 2023). In addition, the PVA/Alg-DA/CA membranes had a more effective inhibitory effect towards *E. coli* than *S. aureus*, possibly because Gram-positive bacteria have thicker cell walls.

### 3.8. *In vivo* wound healing study

The above results demonstrated that the PVA/Alg-DA/CA composite membranes had excellent cytocompatibility along with significant antioxidant activity and antibacterial ability, indicating their great potential for skin wound healing applications. Consequently, we further evaluated the *in vivo* wound healing efficacy of the composite

membranes using a full-thickness skin defect model in mice (Fig. 8a). Specifically, PVA/Alg-DA/CA4 and PVA/Alg-DA/CA8 nanofiber membranes exhibited suitable cell proliferation and outstanding ROS scavenging abilities, were selected as representatives, while PVA and PVA/Alg-DA fiber membranes served as controls. Fig. 8b-d displayed the wound contraction of the blank control, PVA, PVA/Alg-DA, PVA/Alg-DA/CA4, and PVA/Alg-DA/CA8 groups on days 0, 3, 7, and 14, respectively. The results showed that on day 3, all groups experienced a certain degree of wound area reduction, with the PVA/Alg-DA/CA8 group achieving the largest wound contraction of 44.8 %, indicating a higher promotion of wound healing. By day 7, the PVA/Alg-DA, PVA/Alg-DA/CA4, and PVA/Alg-DA/CA8 nanofiber groups outperformed the

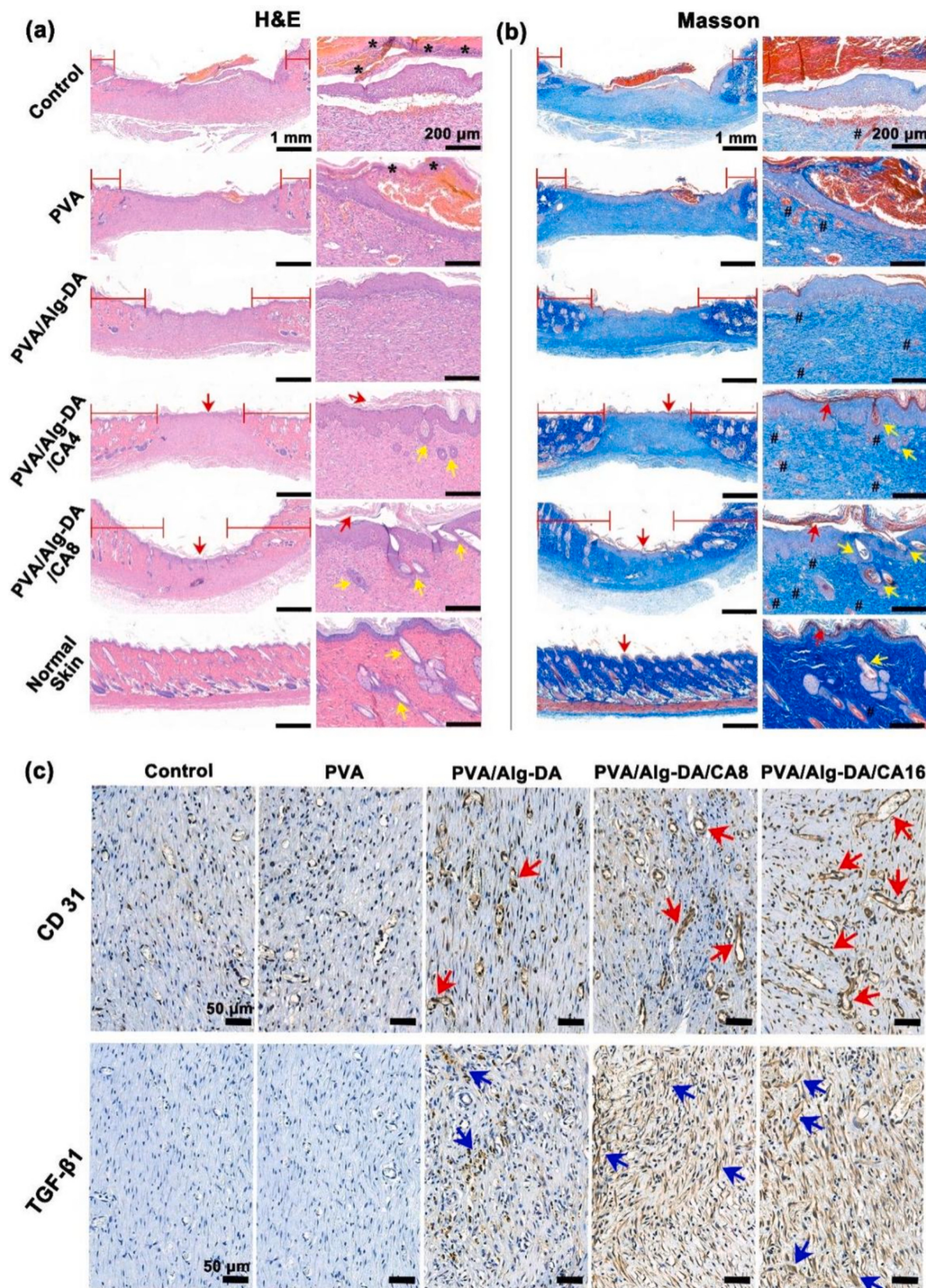


**Fig. 9.** (a) H&E staining images of wounds in different groups. (b) Masson staining images of wounds in different groups, where the red arrow represents finished epithelium, the yellow arrow represents hair follicles, \* represents inflammatory cells, and # represents new blood vessels. (c) IHC staining images of CD31 and TGF- $\beta$ 1 on wound surface in different groups, where the red arrow represents new blood vessels, and the brown-yellow granular or linear sediment indicated by the green arrow represents positive expression of TGF- $\beta$ 1.

blank control and PVA groups, with wound healing rates reaching 41.5 %, 70.7 %, and 76.7 %, respectively. Notably, a higher CA concentration correlated with faster wound recovery. On day 14, wounds in the PVA/Alg-DA/CA4 and PVA/Alg-DA/CA8 nanofiber groups were nearly healed, while the blank control and PVA groups still had 23.1 % and 25.1 % of the wound area remaining, respectively. These quantitative data suggested that PVA/Alg-DA/CA4 and PVA/Alg-DA/CA8 nanofiber membranes exhibit superior wound healing efficacy compared to PVA/Alg-DA, PVA, and the blank control. On the other hand, the wound healing effect of PVA/Alg-DA group was superior to that of the control group and PVA group in the whole treatment stage, which was mainly attributed to the synergistic effects of the nanofiber structure, Alg and DA. In conclusion, these results highlighted the exceptional pro-healing effect of the PVA/Alg-DA/CA8 composite membranes, and the mechanism of wound healing was then investigated by histological analysis in the next section.

### 3.9. Histological analysis of wound regeneration

To further evaluate the skin wound repair process, histopathological studies were performed by H&E and Masson staining. As shown in Fig. 9a and b, after 14 d of treatment, the wound healing of the blank control group and PVA group was poor, with fewer new blood vessels and a large number of inflammatory cells around the wound. In contrast, the PVA/Alg-DA group showed relatively more blood vessels and fewer inflammatory cells in the newly formed skin tissue, which was mainly related to the effect of Alg and DA. Notably, compared to the control, PVA, and PVA/Alg-DA groups, the PVA/Alg-DA/CA4 and PVA/Alg-DA/CA8 membranes significantly enhanced angiogenesis in the new skin tissue, with the formation of bud-like structures, sebaceous glands, and hair follicles, resembling the overall structure of normal skin. Furthermore, the re-epithelialization effect of PVA/Alg-DA/CA groups were evident through measuring the total length of the new epithelium. The wounds treated with PVA/Alg-DA/CA4 and PVA/Alg-DA/CA8 composite membranes were completely covered by new epithelium, whereas the epithelial tissue remained incomplete in the central regions of wounds treated with other fiber membranes. It has been well-established that collagen contributes to wound regeneration (Zhang, Yang, et al., 2024). Masson staining images further indicated that the PVA/Alg-DA/CA4 and PVA/Alg-DA/CA8 treated skin tissues exhibited more collagen deposition, with the collagen fibers being denser and more regularly arranged than those in the other groups. These results provided that PVA/Alg-DA/CA could better promote wound healing through the acceleration on epithelialization and collagen deposition.

Besides collagen deposition, angiogenesis is also crucial for wound healing because blood vessels supplies oxygen, nutrients, and various growth factors to cells surrounding the wound (Peng et al., 2023). Angiogenic disruption significantly impedes the wound healing process. To further evaluate the angiogenesis effect of PVA/Alg-DA/CA membranes, IHC staining of CD31 was performed. CD31 is a transmembrane protein that is expressed during early angiogenesis, thus its expression can be evaluated to account for newly formed blood vessels (Shao et al., 2023). As shown in Fig. 9c, wounds treated with PVA/Alg-DA, PVA/Alg-DA/CA4, and PVA/Alg-DA/CA8 nanofiber membranes exhibited significantly higher levels of CD31 expression compared to the untreated control and wounds treated with PVA alone. However, compared to the PVA/Alg-DA group, the PVA/Alg-DA/CA composite nanofibers demonstrated larger vessel sizes, more defined luminal structures, and a notable increase in the number of blood vessels. These findings suggested that the PVA/Alg-DA/CA possessed excellent pro-vascularization capability.

TGF- $\beta$ 1, a multifunctional growth factor released by fibroblasts, is reported to have the broadest effects and is involved in almost all stages of wound healing (Deng et al., 2024). TGF- $\beta$ 1 can promote the recruitment of inflammatory cells, enhance macrophage-mediated tissue debris clearance, facilitate angiogenesis, aid in re-epithelialization, and

increase collagen deposition during the proliferative phase (Caiado et al., 2011). Existing studies have confirmed that the upregulation of TGF- $\beta$ 1 significantly enhances wound healing rates (Atiba et al., 2011). Therefore, in this study, the expression of TGF- $\beta$ 1 was further detected by IHC staining. As shown in Fig. 9c, on the 14th day of wound healing, the expression of TGF- $\beta$ 1 in wound treated by PVA/Alg-DA/CA4 and PVA/Alg-DA/CA8 nanofiber membrane was significantly higher than that in the PVA/Alg-DA treatment group, while almost no expression was found in the blank control group and PVA group. These data suggested that PVA/Alg-DA/CA treatment could markedly upregulate TGF- $\beta$ 1 protein expression, which might underlie the enhanced collagen deposition.

Collectively, these results signified that the developed PVA/Alg-DA/CA composite membranes markedly bolstered *in vivo* tissue regeneration, presenting enhanced re-epithelialization, collagen deposition, and angiogenesis. This result could be attributed to the synergistic effect of many factors. Firstly, effective deep transdermal delivery by PVA/Alg-DA/CA nanofiber membranes ensured a sustained release of CA and improved its bioavailability. Secondly, the comprehensive attributes of CA including antibacterial, antioxidant, anti-inflammatory and angiogenic capabilities worked in concert to promote wound healing. Thirdly, PVA/Alg-DA/CA nanofiber membranes showed excellent water absorption and permeation properties, which could absorb excess tissue penetrant fluid on the wound surface and provide a proper gas exchange for wound healing. Meanwhile, the high porosity of membranes allowed for the exchange of oxygen and nutrients necessary for wound healing and provided ample space for cell proliferation and migration. The prepared composite membranes were consistent with the characteristics of a good wound dressing, which provided a good physical environment for tissue regeneration. Overall, this study laid a solid foundation for CA-based wound healing formulations, advancing the clinical application of traditional Chinese medicinal herbs in tissue regeneration. This multifunctional electrospun nanofiber dressing developed in this study presents a promising strategy to expedite the healing of full-thickness skin wound through its multifunctional therapeutic attributes.

## 4. Conclusion

In this study, we successfully fabricated PVA/Alg-DA/CA composite nanofiber membranes using Alg-DA conjugates and CA as active ingredients, with PVA serving as the carrier polymer, through the electrospinning technique. These membranes exhibited exceptional biocompatibility, antioxidant properties, and angiogenic potential. Specifically, they supported the adhesion, spreading, and proliferation of fibroblasts *in vitro*, and their antioxidant capabilities effectively protected cells from oxidative damage. In a mouse model of full-thickness skin defects, the functionalized nanofiber membranes significantly promoted neovascularization and tissue remodeling, as evidenced by increased expression of CD31 and TGF- $\beta$ 1 proteins, ultimately accelerating wound healing. The PVA/Alg-DA/CA composite nanofiber membrane emerged as a promising biomaterial platform with great potential for applications in wound repair and healing.

## CRediT authorship contribution statement

**Meng Zhang:** Writing – original draft, Visualization, Validation, Investigation, Formal analysis, Data curation, Conceptualization. **Yinchuan Wang:** Investigation, Conceptualization. **Xueling Yin:** Visualization, Validation. **Mei Xue:** Validation, Data curation. **Xin Zhao:** Validation. **Runxiao Zheng:** Formal analysis, Data curation. **Jianfeng Qiu:** Methodology, Conceptualization. **Zhihong Zhu:** Writing – review & editing, Supervision, Funding acquisition, Conceptualization.

## Declaration of competing interest

The authors declare that they have no known competing financial

interests or personal relationships that could have appeared to influence the work reported in this paper.

## Acknowledgements

This work was financially supported by the National Natural Science Foundation of China (No. 52072139), the Natural Science Foundation of Hubei Province (No. 2019CFB606), the Basic Scientific Research Foundation of Central China Normal University (No. CCNU24JCPT008), the Academic Promotion Program of Shandong First Medical University (No. 2019QL009), and the Science and Technology from Jinan (No. 2020GXRC018).

## Appendix A. Supplementary data

Supplementary data to this article can be found online at <https://doi.org/10.1016/j.carbpol.2025.123298>.

## Data availability

Data will be made available on request.

## References

- Ahn, S., Ardon, H. A. M., Campbell, P. H., Gonzalez, G. M., & Parker, K. K. (2019). Alfalfa nanofibers for dermal wound healing. *ACS Applied Materials & Interfaces*, 11(37), 33535–33547.
- Al Horani, R. Z., Kepkeci, R. A., & Icoglu, H. I. (2024). Bioactive PVA nanofiber mat loaded with artichoke bracts extract as a promising wound dressing biomaterial. *Materials Today Communications*, 38, Article 108249.
- Atiba, A., Nishimura, M., Kakinuma, S., Hiraoka, T., Goryo, M., Shimada, Y., ... Uzuka, Y. (2011). Aloe vera oral administration accelerates acute radiation-delayed wound healing by stimulating transforming growth factor- $\beta$  and fibroblast growth factor production. *American Journal of Surgery*, 201(6), 809–818.
- Blanquer, A., Kostakova, E. K., Filova, E., Lisenko, M., Broz, A., Mullerova, J., ... Jencova, V. (2024). A novel bifunctional multilayered nanofibrous membrane combining polycaprolactone and poly (vinyl alcohol) enriched with platelet lysate for skin wound healing. *Nanoscale*, 16(4), 1924–1941.
- Caiado, F., Carvalho, T., Silva, F., Castro, C., Clode, N., Dye, J. F., & Dias, S. (2011). The role of fibrin E on the modulation of endothelial progenitors adhesion, differentiation and angiogenic growth factor production and the promotion of wound healing. *Biomaterials*, 32(29), 7096–7105.
- Chai, C., Zhang, P., Ma, L., Fan, Q., Liu, Z., Cheng, X., ... Hao, J. (2023). Regenerative antibacterial hydrogels from medicinal molecule for diabetic wound repair. *Bioactive Materials*, 25, 541–554.
- De Silva, R. T., Dissanayake, R. K., Mantilaka, M. M. M. G. P. G., Wijesinghe, W. P. S. L., Kaleel, S. S., Premachandra, T. N., ... de Silva, K. M. N. (2018). Drug-loaded halloysite nanotube-reinforced electrospun alginate-based nanofibrous scaffolds with sustained antimicrobial protection. *ACS Applied Materials & Interfaces*, 10(40), 33913–33922.
- Deng, Z. Q., Fan, T., Xiao, C., Tian, H., Zheng, Y. J., Li, C. X., & He, J. (2024). TGF- $\beta$  signaling in health, disease, and therapeutics. *Signal Transduction and Targeted Therapy*, 9(1), 61.
- Destaye, A. G., Lin, C.-K., & Lee, C.-K. (2013). Glutaraldehyde vapor cross-linked nanofibrous PVA mat with in situ formed silver nanoparticles. *ACS Applied Materials & Interfaces*, 5(11), 4745–4752.
- Ding, Q., Ding, C., Liu, X., Zheng, Y., Zhao, Y., Zhang, S., ... Liu, W. (2023). Preparation of nanocomposite membranes loaded with taxifolin liposome and its mechanism of wound healing in diabetic mice. *International Journal of Biological Macromolecules*, 241, Article 124537.
- Dong, Y., & Wang, Z. (2023). ROS-scavenging materials for skin wound healing: Advancements and applications. *Frontiers in Bioengineering and Biotechnology*, 11, Article 1304835.
- Doostan, M., Doostan, M., Mohammadi, P., Khoshnevisan, K., & Maleki, H. (2023). Wound healing promotion by flaxseed extract-loaded polyvinyl alcohol/chitosan nanofibrous scaffolds. *International Journal of Biological Macromolecules*, 228, 506–516.
- Fadilah, N. I. M., Phang, S. J., Kamaruzaman, N., Salleh, A., Zawani, M., Sanyal, A., ... Faizi, M. B. (2023). Antioxidant biomaterials in cutaneous wound healing and tissue regeneration: A critical review. *Antioxidants*, 12(4), 787.
- Ghorbani, M., Ercole, F., Nazemi, K., Warne, N. M., Quinn, J. F., & Kempe, K. (2024). A comparative study on surface-engineered nanoceria using a catechol copolymer design: Colloidal stability vs. antioxidant activity. *Nanoscale*, 16(36), 17024–17041.
- Gómez-Ordóñez, E., & Rupérez, P. (2011). FTIR-ATR spectroscopy as a tool for polysaccharide identification in edible brown and red seaweeds. *Food Hydrocolloids*, 25(6), 1514–1520.
- Han, X., Saengow, C., Ju, L., Ren, W., Ewoldt, R. H., & Irudayaraj, J. (2024). Exosome-coated oxygen nanobubble-laden hydrogel augments intracellular delivery of exosomes for enhanced wound healing. *Nature Communications*, 15(1), Article 3435.
- Huang, H., Chen, L., Hou, Y., He, W., Wang, X., Zhang, D., & Hu, J. (2023). Self-assembly of chlorogenic acid into hydrogel for accelerating wound healing. *Colloids and Surfaces B-Biointerfaces*, 228, Article 113440.
- Huang, H., Liao, S., Zhang, D., Liang, W., Xu, K., Zhang, Y., & Lang, M. (2024). A macromolecular cross-linked alginate aerogel with excellent concentrating effect for rapid hemostasis. *Carbohydrate Polymers*, 338, Article 122148.
- Huang, J., Chen, G., Han, T., Yi, C., Zhang, Y., Ding, L., ... Zhou, S. (2023). Ultrafast and facile construction of programmable, multidimensional wrinkled-patterned polyacrylamide/sodium alginate hydrogels for human skin-like tactile perception. *Carbohydrate Polymers*, 319, Article 121196.
- Huang, Z., An, H., Guo, H. T., Ji, S., Gu, Q., Gu, Z., & Wen, Y. Q. (2024). An asymmetric natural nanofiber with rapid temperature responsive detachability inspired by *Andrias davidianus* for full-thickness skin wound healing. *Advanced Fiber Materials*, 6(2), 473–488.
- Hunt, M., Torres, M., Bachar-Wikstrom, E., & Wikstrom, J. D. (2024). Cellular and molecular roles of reactive oxygen species in wound healing. *Communications Biology*, 7(1), Article 1534.
- Jiang, Z., Zheng, Z., Yu, S., Gao, Y., Ma, J., Huang, L., & Yang, L. (2023). Nanofiber scaffolds as drug delivery systems promoting wound healing. *Pharmaceutics*, 15(7), Article 1829.
- Kumar, A., Ryparova, P., Hosseinpouria, R., Adamopoulos, S., Prosek, Z., Zigon, J., & Petric, M. (2019). Hydrophobicity and resistance against microorganisms of heat and chemically crosslinked poly(vinyl alcohol) nanofibrous membranes. *Chemical Engineering Journal*, 360, 788–796.
- Li, P., Tan, D., Su, A., Xiong, X., Gao, S., Zhang, H., ... Jiang, Q. (2025). Gallic acid functionalized silk fibroin/gelatin composite wound dressing for enhanced wound healing. *Biomedical Materials*, 20(1), Article 015002.
- Liu, T., Wang, Y., Liu, J., Han, X., Zou, Y., Wang, P., ... Zhang, X. (2024). An injectable photocuring silk fibroin-based hydrogel for constructing an antioxidant microenvironment for skin repair. *Journal of Materials Chemistry B*, 12(9), 2282–2293.
- Luo, Y., Wei, X., Wan, Y., Lin, X., Wang, Z., & Huang, P. (2019). 3D printing of hydrogel scaffolds for future application in photothermal therapy of breast cancer and tissue repair. *Acta Biomaterialia*, 92, 37–47.
- Nematollahi, S., Maghsoudian, S., Motasadizadeh, H., Nouri, Z., Azad, K., Fatahi, Y., ... Dinarvand, R. (2025). Polyhexamethylene biguanidine coated silver nanoparticles embedded into chitosan thiourea/PVA nanofibers as wound healing mats: In vitro and in vivo studies. *Carbohydrate Polymers*, 347, Article 122704.
- Nezari, S., Sarli, M., Hivechi, A., Bahrami, S. H., Milan, P. B., Latifi, N., ... Gharagheshlagh, S. N. (2023). Investigating the effect of poly ( $\epsilon$ -caprolactone) nanofibers scaffolds with random, unidirectionally, and radially aligned morphologies on the fibroblast cell's attachment and growth behavior. *Turkish Journal of Chemistry*, 47(1), 54–62.
- Peng, H., Li, H. C., Zhang, X., Tang, J. Z., Liang, Y. P., Qiao, L. P., ... Zhang, J. (2023). 3D-exosomes laden multifunctional hydrogel enhances diabetic wound healing via accelerated angiogenesis. *Chemical Engineering Journal*, 475, Article 146238.
- Prakashan, D., Singh, A., Deshpande, A. D., Chandra, V., Sharma, G. T., & Gandhi, S. (2024). Bone marrow derived mesenchymal stem cells enriched PCL-gelatin nanofiber scaffold for improved wound healing. *International Journal of Biological Macromolecules*, 274, Article 133447.
- Qu, M., Xu, W., Zhou, X., Tang, F., Chen, Q., Zhang, X., ... Chen, Q. (2024). An ROS-scavenging treg-recruiting hydrogel patch for diabetic wound healing. *Advanced Functional Materials*, 34(26), Article 2314500.
- Rojas-Gonzalez, A., Yuritzi Figueroa-Hernandez, C., Gonzalez-Rios, O., Leonor Suarez-Quiroz, M., Maria Gonzalez-Amaro, R., Josue Hernandez-Estrada, Z., & Rayas-Duarte, P. (2022). Coffee chlorogenic acids incorporation for bioactivity enhancement of foods: a review. *Molecules*, 27(11), Article 3400.
- Sadeghi-Aghdash, M., Rahimnejad, M., Adeli, H., & Feizi, F. (2024). Catecholamines polymerization crosslinking for alginate-based burn wound dressings developed with ciprofloxacin and zinc oxide interactions. *International Journal of Biological Macromolecules*, 260, Article 129400.
- Sakugawa, K., Ikeda, A., Takemura, A., & Ono, H. (2004). Simplified method for estimation of composition of alginates by FTIR. *Journal of Applied Polymer Science*, 93(3), 1372–1377.
- Seaberg, J., Clegg, J. R., Bhattacharya, R., & Mukherjee, P. (2023). Self-therapeutic nanomaterials: Applications in biology and medicine. *Materials Today*, 62, 190–224.
- Shah, M.-A., Kang, J.-B., Park, D.-J., Kim, M.-O., & Koh, P.-O. (2021). Chlorogenic acid alleviates neurobehavioral disorders and brain damage in focal ischemia animal models. *Neuroscience Letters*, 760, Article 136085.
- Shao, Z. J., Yin, T. Y., Jiang, J. B., He, Y., Xiang, T., & Zhou, S. B. (2023). Wound microenvironment self-adaptive hydrogel with efficient angiogenesis for promoting diabetic wound healing. *Bioactive Materials*, 20, 561–573.
- Song, Y., Liu, C., Xu, X., Ren, L., Zhou, X., Xu, H., ... Wang, Z. (2024). Chitosan-based multifunctional hydrogel with bio-adhesion and antioxidant properties for efficient wound hemostasis. *Colloids and Surfaces B-Biointerfaces*, 234, Article 113697.
- Suarez-Gonzalez, D., Barnhart, K., Saito, E., Vanderby, R., Jr., Hollister, S. J., & Murphy, W. L. (2010). Controlled nucleation of hydroxyapatite on alginate scaffolds for stem cell-based bone tissue engineering. *Journal of Biomedical Materials Research Part A*, 95A(1), 222–234.
- Sun, S., Ding, C., Liu, X., Zhao, Y., Zhang, J., Ding, Q., ... Yang, M. (2022). Silk protein/polyvinylpyrrolidone nanofiber membranes loaded with puerarin accelerate wound healing in mice by reducing the inflammatory response. *Biomaterials Advances*, 135, Article 212734.
- Tordi, P., Gelli, R., Ridi, F., & Bonini, M. (2024). A bioinspired and sustainable route for the preparation of Ag-crosslinked alginate fibers decorated with silver nanoparticles. *Carbohydrate Polymers*, 326, Article 121586.

- Wang, L., Ding, L., Yu, Z., Zhang, T., Ma, S., & Liu, J. (2016). Intracellular ROS scavenging and antioxidant enzyme regulating capacities of corn gluten meal-derived antioxidant peptides in HepG2 cells. *Food Research International*, 90, 33–41.
- Wang, L., Zhao, Z., Dong, J., Li, D., Dong, W., Li, H., ... Deng, B. (2023). Mussel-inspired multifunctional hydrogels with adhesive, self-healing, antioxidative, and antibacterial activity for wound healing. *ACS Applied Materials & Interfaces*, 15(13), 16515–16525.
- Wang, P., Meng, X., Xue, J., Fan, C., & Wang, J. (2023). Genome-wide analysis for nanofiber induced global gene expression profile: A study in MC3T3-E1 cells by RNA-Seq. *Colloids and Surfaces B-Biointerfaces*, 223, Article 113143.
- Wang, S., Ju, J., Wu, S., Lin, M., Sui, K., Xia, Y., & Tan, Y. (2020). Electrospinning of biocompatible alginate-based nanofiber membranes via tailoring chain flexibility. *Carbohydrate Polymers*, 230, Article 115665.
- Wang, X., Sun, K., Wang, C., Yang, M., Qian, K., Ye, B., ... Bai, J. (2025). Ultrasound-responsive microfibers promoted infected wound healing with neuro-vascularization by segmented sonodynamic therapy and electrical stimulation. *Biomaterials*, 313, Article 122803.
- Wang, Y., Zhang, Y., Yang, Y.-P., Jin, M. Y., Huang, S., Zhuang, Z.-M., ... Tan, W.-Q. (2024). Versatile dopamine-functionalized hyaluronic acid-recombinant human collagen hydrogel promoting diabetic wound healing via inflammation control and vascularization tissue regeneration. *Bioactive Materials*, 35, 330–345.
- Wang, Z., An, Z., Richel, A., Huang, M., Gou, X., Xu, D., ... Zhou, X. (2024). Ferrous sulfate remodels the properties of sodium alginate-based hydrogel and facilitates the healing of wound infection caused by MRSA. *Carbohydrate Polymers*, 346, Article 122554.
- Wang, Z., Zhai, X., Sun, Y., Yin, C., Yang, E., Wang, W., & Sun, D. (2020). Antibacterial activity of chlorogenic acid-loaded SiO<sub>2</sub> nanoparticles caused by accumulation of reactive oxygen species. *Nanotechnology*, 31(18), Article 185101.
- Yang, Y., Du, Y., Zhang, J., Zhang, H., & Guo, B. (2022). Structural and functional design of electrospun nanofibers for hemostasis and wound healing. *Advanced Fiber Materials*, 4(5), 1027–1057.
- Zhang, M., Ran, S., Yin, X., Zhang, J., Sun, X., Sun, W., & Zhu, Z. (2023). Mesoporous polydopamine nanoplates loaded with calcium ascorbate for amplified oxidation and photothermal combination cancer therapy. *BMEMAT*, 1(4), Article e12041.
- Zhang, M., Zhang, J., Ran, S., Sun, W., & Zhu, Z. (2022). Polydopamine-assisted decoration of Se nanoparticles on curcumin-incorporated nanofiber matrices for localized synergistic tumor-wound therapy. *Biomaterials Science*, 10(2), 536–548.
- Zhang, Q., Huang, Z., Jiang, H., Wu, M., Chen, F., Zhao, G., & Ma, P. (2025). “Bamboo-like” strong and tough sodium alginate/polyacrylate hydrogel fiber with directional controlled release for wound healing promotion. *Carbohydrate Polymers*, 347, Article 122761.
- Zhang, T., Huang, Y., Gong, Y., Shi, X., Xiao, D., Ren, L., ... Zhao, C. (2024). A ROS-responsive and scavenging hydrogel for postoperative abdominal adhesion prevention. *Acta Biomaterialia*, 184, 98–113.
- Zhang, W. B., Wu, W. W., Wang, T., Wu, Z. W., Li, Y., Ding, T., ... Huang, F. (2024). Novel supramolecular hydrogel for infected diabetic foot ulcer treatment. *Advanced Healthcare Materials*. <https://doi.org/10.1002/adhm.202402092>
- Zhang, X., Yang, C., Zeng, X., & Li, G. (2024). A bioactive composite sponge based on biomimetic collagen fibril and oxidized alginate for noncompressible hemorrhage and wound healing. *Carbohydrate Polymers*, 343, Article 122409.
- Zhong, H., Fang, Y., Luo, M., Wang, L., Huang, J., Dai, G., ... Du, J. (2024). Deferoxamine-loaded injectable chitosan-grafted chlorogenic acid/oxidized hyaluronic acid hybrid hydrogel with antibacterial, anti-inflammatory, and angiogenesis-promoting properties for diabetic wound repair. *ACS Applied Materials & Interfaces*, 16(22), 28209–28221.
- Zhou, Z., Mei, X., Hu, K., Ma, M., & Zhang, Y. (2023). Nano-hybrid double network hydrogels based on a platinum nanzyme composite for antimicrobial and diabetic wound healing. *ACS Applied Materials & Interfaces*, 15(14), 17612–17626.